TU Delft

Delft University of Technology

Document Version
Final published version

Citation (APA)
Zhang, W., Zhang, K., & Al Kobaisi, M. (2025). Impact of grid non-K-orthogonality on CO_2 migration and pressure prediction using two-point and multi-point flux approximation methods. *Physics of Fluids*, *37*(8), Article 083421. https://doi.org/10.1063/5.0282130

Important note
To cite this publication, please use the final published version (if applicable).
Please check the document version above.

Copyright
In case the licence states “Dutch Copyright Act (Article 25fa)”, this publication was made available Green Open Access via the TU Delft Institutional Repository pursuant to Dutch Copyright Act (Article 25fa, the Taverne amendment). This provision does not affect copyright ownership.
Unless copyright is transferred by contract or statute, it remains with the copyright holder.

Sharing and reuse
Other than for strictly personal use, it is not permitted to download, forward or distribute the text or part of it, without the consent of the author(s) and/or copyright holder(s), unless the work is under an open content license such as Creative Commons.

Takedown policy
Please contact us and provide details if you believe this document breaches copyrights.
We will remove access to the work immediately and investigate your claim.

This work is downloaded from Delft University of Technology.

Green Open Access added to TU Delft Institutional Repository
as part of the Taverne amendment.

More information about this copyright law amendment
can be found at https://www.openaccess.nl.

Otherwise as indicated in the copyright section:
the publisher is the copyright holder of this work and the
author uses the Dutch legislation to make this work public.

Physics of Fluids

RESEARCH ARTICLE | AUGUST 27 2025

Impact of grid non-K-orthogonality on CO_2 migration and pressure prediction using two-point and multi-point flux approximation methods

Wenjuan Zhang ; Kai Zhang ; Mohammed Al Kobaisi

Check for updates

Physics of Fluids 37, 083421 (2025)
https://doi.org/10.1063/5.0282130

View Online
Export Citation

Articles You May Be Interested In

Numerical simulation of two-phase flow in zoned reservoirs based on a hybrid method combining the two-point flux approximation and the mimetic finite difference method

Physics of Fluids (June 2025)

A novel streamline simulation method for fractured reservoirs with full-tensor permeability

Physics of Fluids (January 2024)

A hybrid method of mimetic finite difference and discontinuous Galerkin for flow problems in polymer flooding reservoirs

Physics of Fluids (June 2025)

04 September 2025 09:47:42

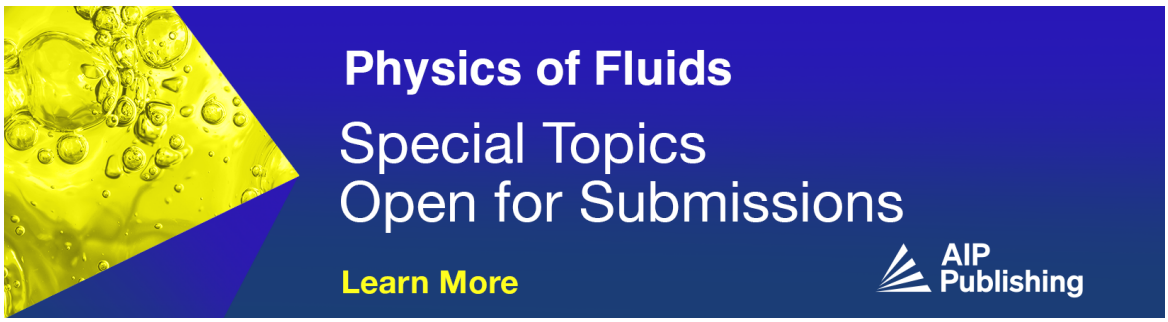

AIP Publishing

Physics of Fluids ARTICLE pubs.aip.org/aip/pof

Impact of grid non-K-orthogonality on CO_2 migration and pressure prediction using two-point and multi-point flux approximation methods

Cite as: Phys. Fluids **37**, 083421 (2025); doi: 10.1063/5.0282130
Submitted: 23 May 2025 · Accepted: 4 August 2025 ·
Published Online: 27 August 2025

View Online Export Citation CrossMark

Wenjuan Zhang,[1] Kai Zhang,[1,a)] and Mohammed Al Kobaisi[2,3]

AFFILIATIONS

[1]School of Civil Engineering, Qingdao University of Technology, Qingdao 266520, China
[2]Department of Chemical and Petroleum Engineering, Khalifa University of Science and Technology, Abu Dhabi, United Arab Emirates
[3]Delft Institute of Applied Mathematics, Delft University of Technology, Delft, The Netherlands

[a)]**Author to whom correspondence should be addressed:** zhangkai@qut.edu.cn

ABSTRACT

Accurate simulation of multiphase flow is essential for predicting pressure buildup and CO_2 plume migration in geological carbon storage. The two-point flux approximation (TPFA) method is widely used in reservoir simulation due to its simplicity, but it is only consistent on K-orthogonal grids. Realistic subsurface models, however, often involve non-K-orthogonal grids caused by geological features such as faults and fractures, where TPFA may introduce significant errors. This study systematically quantifies the numerical error associated with using TPFA on non-K-orthogonal grids in the context of CO_2 storage in saline aquifers. Based on the formalism of the TPFA method, a numerical index is proposed in this work for the first time to quantify the degree of grid non-K-orthogonality. A series of numerical experiments are presented to compare the TPFA and multi-point flux approximation (MPFA) methods, with high-resolution reference solutions used as benchmarks. Results show that grid non-K-orthogonality can impact the accuracy of both TPFA and MPFA solutions with larger degree of grid non-K-orthogonality leading to larger solution errors in general. The magnitude of solution errors of the MPFA method is significantly smaller than that of TPFA in terms of both pressure solution and CO_2 saturation as it is much more robust against grid non-K-orthogonality effect. In particular, the TPFA method can produce substantial deviations in CO_2 saturation distributions when grid non-K-orthogonality is present, indicating the necessity of more advanced discretization methods such as MPFA for modeling the CO_2 plume migration behavior more accurately. These findings highlight the importance of selecting appropriate discretization methods for geologically complex reservoirs and the proposed grid non-K-orthogonality index can help evaluate the solution accuracy in a general simulation study. Our results offer practical guidance on the tradeoffs between computational efficiency and physical accuracy in carbon storage modeling.

Published under an exclusive license by AIP Publishing. https://doi.org/10.1063/5.0282130

04 September 2025 09:47:42

I. INTRODUCTION

Hydrocarbon resources such as oil and natural gas are expected to remain integral to the global energy mix for the foreseeable future, even as the world advances toward a fully sustainable energy system. In this transitional period, carbon capture and storage (CCS) has emerged as a critical strategy for mitigating CO_2 emissions associated with the combustion of fossil fuels. Among the various CCS approaches, geological storage of carbon dioxide in deep saline aquifers has garnered considerable attention due to the widespread availability and significant storage capacity of these formations. Accurate numerical simulation plays a critical role in designing, operating, and regulating such storage projects and in advancing our understanding of multiphase flow in porous media.[1] It enables the evaluation of storage capacity, pressure buildup, and plume migration under a wide range of geological and operational conditions. For example, a numerical simulation model of CO_2 storage in deep saline aquifers has been used to analyze the influence of reservoir physical properties on plume migration and storage capacity, showing that permeability and depth strongly affect CO_2 distribution, while porosity and temperature have minor effects.[2] Long-term simulation of field-scale storage projects, such as Sleipner, has been used to track CO_2 plume evolution and assess the reliability of monitoring techniques over decades.[3] In fractured or geologically complex formations, numerical models incorporating fracture networks have been applied to simulate multiphase

Published under an exclusive license by AIP Publishing

flow and evaluate injection efficiency.[4] Simulations are also commonly used to compare different injection scenarios and quantify the dynamic behavior of CO_2 under various structural configurations, such as in the Choszczno-Suliszewo structure in Poland.[5] Other studies focus on predicting storage efficiency and maximum migration distance as functions of permeability and boundary conditions.[6] Recently, hybrid approaches combining numerical simulation with machine learning have emerged to improve the reliability and scalability of long-term CO_2 storage predictions.[7] In addition, with growing interest in accelerating CO_2 storage optimization and uncertainty quantification, numerical simulation is increasingly being used to generate large-scale training datasets for surrogate models and machine learning frameworks that approximate full-physics behavior at significantly lower computational cost.[8–10] Collectively, these efforts demonstrate the breadth of simulation-based research in CO_2 storage and underscore its importance in both scientific analysis and engineering design.

Many of the numerical simulation approaches used in CO_2 storage studies rely on the two-point flux approximation (TPFA) method to discretize the governing flow equations. TPFA is widely adopted due to its simplicity, computational efficiency, and compatibility with standard reservoir simulation software.[11] However, its accuracy depends on a restrictive assumption: the simulation grid must be K-orthogonal, meaning that the grid lines must align with the principal directions of the permeability tensor. In real-world applications, this condition is often violated due to the need to conform grids to complex geological features such as dipping layers, faults, and fractures. When applied to non-K-orthogonal grids, TPFA can produce significant numerical errors in both pressure and flux calculations, potentially leading to inaccurate predictions of CO_2 plume migration, pressure buildup, and trapping efficiency. These limitations are particularly critical in storage sites where geological complexity plays a dominant role in flow behavior. In Ref. 12 the authors investigated the effect of grid shape and resolution on the simulation results of geological storage of CO_2 and found that high-resolution Voronoi tessellation can reduce the grid-orientation effect significantly, but the study stops short of quantifying the numerical errors. Despite its effectiveness in reducing grid-orientation effect, the Voronoi grid cannot guarantee grid-K-orthogonality in general simulation settings, especially for anisotropic permeability tensors, and the accuracy of TPFA solutions will be compromised. To quantify the errors, various measures were proposed in the literature to evaluate the grid quality.[13,14] When the grid is K-orthogonal, for any face in the grid, the angle between the co-normal vector (defined as the product of the cell permeability tensor and the face normal) and the vector connecting the cell centroid to the face centroid is 0. A larger angle means a higher degree of grid non-K-orthogonality. Therefore, the grid quality measures often involve some form of the angle or the sine of the angle. Since using the angle (or sine of the angle) alone does not give a direct indication of the magnitude of the relative errors when the flux through the face is approximated, the predictive power of the grid quality measures may be limited.

On the other hand, the geological models are often built with the aim of characterizing the geometry of the geological features as accurately as possible and highly flexible grids such as the corner-point grid format[15] is mostly adopted in the geoscience community. As a result, the simulation engineer often does not have the freedom to choose the best grid format from the numerical simulation perspective but have to work with non-K-orthogonal and sometimes highly deviated grids. Therefore, more accurate but computationally intensive methods have been proposed as alternatives to TPFA method for handling general grid geometries and full-tensor permeabilities such as the multi-point flux approximation (MPFA),[16–18] the mimetic finite difference method,[19,20] the nonlinear finite volume method.[21,22] Despite these advances, TPFA remains dominant in CO_2 storage simulations because of its robustness and computational efficiency, and there is a lack of systematic investigation into the quantitative errors it introduces in non-ideal grid settings, especially in the context of CO_2 storage in saline aquifers.

In this work, we aim to systematically quantify the numerical errors introduced by the TPFA method when applied to non-K-orthogonal grids in the context of CO_2 storage simulation. To this end, we conduct a series of controlled numerical experiments comparing the TPFA and MPFA discretization schemes against high-fidelity reference solutions. The comparison focuses on key performance indicators including pressure distribution and CO_2 plume migration patterns. By isolating the impact of grid non-orthogonality and reservoir heterogeneity, our study provides practical insights into when TPFA may be insufficient and whether the added computational cost of MPFA is justified. Moreover, considering the inadequacy of the existing grid-K-orthogonality measures, we propose a new numerical index for evaluating the degree of grid-K-orthogonality. The new index is based on the derivation of the TPFA formulation and it quantifies the relative magnitude of the flux approximation errors of the TPFA method. Numerical experiments demonstrate that our new grid-K-orthogonality measure has reasonably good predictive capability. The results are intended to guide modelers and engineers in choosing appropriate numerical methods for reliable prediction of CO_2 behavior in geologically complex storage formations. The rest of the paper is organized as follows: the mathematical model governing CO_2-water two phase flow will be briefly reviewed in the next section, followed by a description of the numerical discretization methods and the proposed numerical index for quantifying grid non-K-orthogonality in Sec. III. Numerical experiments setup and simulation results are detailed in Sec. IV and finally Sec. V concludes this paper.

II. MATHEMATICAL MODEL

We consider the problem of simulating immiscible two phase (supercritical CO_2 and resident water) flow in a slightly compressible porous media. The CO_2 phase is non-wetting and the water phase is wetting. The two phases are denoted by g and w, respectively. The mass conservation equation is written for each phase $\alpha = g, w$ as[11]

$$\frac{\partial}{\partial t}(\phi \rho_\alpha S_\alpha) + \nabla \cdot (\rho_\alpha \mathbf{v}_\alpha) = \rho_\alpha q_\alpha. \tag{1}$$

Here, ϕ is porosity, ρ_α is mass density of phase α, S_α is phase saturation, $\mathbf{v}_\alpha$ is phase velocity and q_α is phase volumetric source/sink terms. The phase velocity is related to the phase pressure p_α by Darcy's law

$$\mathbf{v}_\alpha = -\frac{k_{r\alpha}}{\mu_\alpha}\mathbf{K}(\nabla p_\alpha - \gamma_\alpha \nabla D) = -\lambda_\alpha \mathbf{K}(\nabla p_\alpha - \gamma_\alpha \nabla D), \tag{2}$$

where $\mathbf{K}$ is the absolute permeability tensor, and $k_{r\alpha}$, μ_α, γ_α, and λ_α are phase relative permeability, phase viscosity, phase specific weight and phase mobility, respectively. The phase specific weight is simply the

04 September 2025 09:47:42

Published under an exclusive license by AIP Publishing

product of phase density and gravity constant and D is depth. The system is complemented by the following constraints

$$\begin{aligned} S_w + S_g &= 1\,, \\ p_g - p_w &= p_c(S_w), \end{aligned} \tag{3}$$

where $p_c(Sw)$ denotes the capillary pressure between the two phases. The mathematical model is closed with appropriate initial and boundary conditions.

III. NUMERICAL METHODS

A. Numerical discretization

The mathematical model was solved fully implicitly, using a finite volume method for spatial discretization (TPFA or MPFA) and the backward Euler method for time integration. The discrete form of the mass conservation equation for an arbitrary cell Ω_i reads as follows[11]

$$\frac{V_i}{\Delta t}\left[(\phi\rho_\alpha S_\alpha)_i^{n+1} - (\phi\rho_\alpha S_\alpha)_i^{n}\right] + \sum_{j\in\mathcal{N}_i} F_{\alpha,ij}^{n+1} - Q_{\alpha,i}^{n+1} = 0, \tag{4}$$

where V_i is the bulk volume of cell Ω_i,and Δt is the time step size. The superscripts n and $n+1$ denote the current time step and the next time step, respectively. $\mathcal{N}_i$ is the set of neighboring cells sharing a common face with cell Ω_i. $F_{\alpha,ij}$ is the numerical mass flux flowing from cell Ω_i to neighboring cell Ω_j and $Q_{\alpha,i}$ is the integrated source term. The numerical mass flux is given by

$$F_{\alpha,ij}^{n+1} \approx \int_{\Gamma_{ij}} \rho_\alpha^{n+1}\mathbf{v}_\alpha^{n+1}\cdot\mathbf{n}dS, \tag{5}$$

where Γ_{ij} denotes the face shared by cell Ω_i and Ω_j and $\mathbf{n}$ is the unit normal pointing outward of cell Ω_i. Inserting Darcy's equation (2) into the above equation leads to

$$\begin{aligned} F_{\alpha,ij}^{n+1} &\approx \int_{\Gamma_{ij}} -\rho_\alpha^{n+1}\lambda_\alpha^{n+1}\mathbf{K}\left(\nabla p_\alpha^{n+1} - \gamma_\alpha^{n+1}\nabla D\right)\cdot\mathbf{n}dS \\ &= (\rho_\alpha\lambda_\alpha)_{ij}^{n+1}\int_{\Gamma_{ij}} -\mathbf{K}\left(\nabla p_\alpha^{n+1} - \gamma_\alpha^{n+1}\nabla D\right)\cdot\mathbf{n}dS. \end{aligned} \tag{6}$$

Where the product of phase density and mobility on the interface is approximated by the single-point upstream weighting. The difference between TPFA and MPFA method lies in the approximation of the surface integration $\int_{\Gamma_{ij}} -\mathbf{K}\left(\nabla p_\alpha^{n+1} - \gamma_\alpha^{n+1}\nabla D\right)\cdot\mathbf{n}dS$. The TPFA method[23] approximates this integral by using the pressure unknowns associated with the two cells Ω_i and Ω_j that share the interface Γ_{ij}. As for MPFA method, there are different variants such as the MPFA-O method,[16] MPFA-Z method,[24] MPFA-L method[25] and more advanced versions.[18,26,27] In this work, we implemented the classical MPFA-O method and the implementation details follows the formulation presented in Ref. 28. For completeness, a brief introduction to the TPFA and MPFA-O formulation for approximating the surface integral $\int_{\Gamma_{ij}} -\mathbf{K}\nabla\boldsymbol{p}\cdot\mathbf{n}dS$ is given here. Consider an internal face shared by two cells Ω_i and Ω_j shown in Fig. 1. The centroids of the two cells are denoted by $\mathbf{x}_i$ and $\mathbf{x}_j$, respectively, and $\mathbf{x}_f$ is the face centroid. The vector $\mathbf{d}_{i,j}$ is defined as $\mathbf{d}_{i,j} = \mathbf{x}_f - \mathbf{x}_i$. The unit normal vector to the face is denoted by $\mathbf{n}_{i,j}$ and it points out of cell Ω_i. Assuming a linearly varying pressure inside each cell, the TPFA method approximates the flux flowing out of cell Ω_i through the face as

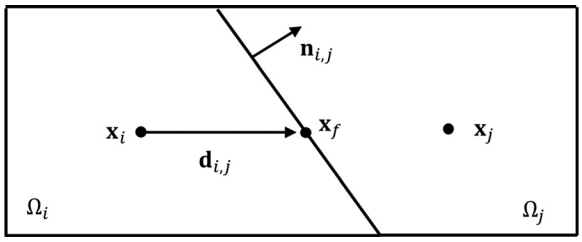

FIG. 1. Schematic of TPFA formulation.

$$F_{i,j} = A_{i,j}\mathbf{K}_i\frac{p_i - p_f}{\|\mathbf{d}_{i,j}\|^2}\mathbf{d}_{i,j}\cdot\mathbf{n}_{i,j} = T_{i,j}(p_i - p_f), \tag{7}$$

where $A_{i,j}$ is the face area and $\mathbf{K}_i$ is the constant permeability tensor of cell Ω_i. p_i and p_f are pressures at points $\mathbf{x}_i$ and $\mathbf{x}_f$, respectively. Finally, $T_{i,j}$ is the so-called one-sided transmissibility as it is computed by using information of cell Ω_i only. The flux flowing out of cell Ω_j through the face can be calculated analogously as

$$F_{j,i} = T_{j,i}(p_j - p_f). \tag{8}$$

The pressure p_f is then solved by imposing the flux continuity condition $F_{i,j} + F_{j,i} = 0$ on the face and the final flux proximation is given by

$$F_{i,j} = -F_{j,i} = \left(T_{i,j}^{-1} + T_{j,i}^{-1}\right)^{-1}(p_i - p_j) = T_{ij}(p_i - p_j), \tag{9}$$

where T_{ij} is the transmissibility associated with the face connecting the cell Ω_i and Ω_j.

To determine the transmissibility coefficients using the MPFA-O formulation, consider four cells that share a common vertex O shown in Fig. 2. The cells are numbered locally as 1–4. First, an interaction region is formed around the vertex by connecting the centroids of the cells with the centroids (A, B, C, D) of the faces connected to the vertex O. The interaction region is composed of four sub-regions belonging to the four cells. The four half faces OA, OB, OC, and OD are called sub-interfaces. The MPFA-O method seeks to determine fluxes through these sub-interfaces first and subsequently the flux through a whole interface can be obtained by assembling fluxes through the respective two sub-interfaces constituting the whole interface. Introducing pressure at the four faces centroids as auxiliary unknowns and assuming a linearly varying pressure over each sub-region, the pressure gradient over a sub-region can be calculated using pressure at

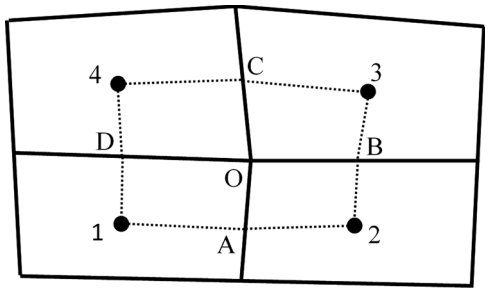

FIG. 2. Schematic of MPFA-O formulation.

04 September 2025 09:47:42

Published under an exclusive license by AIP Publishing

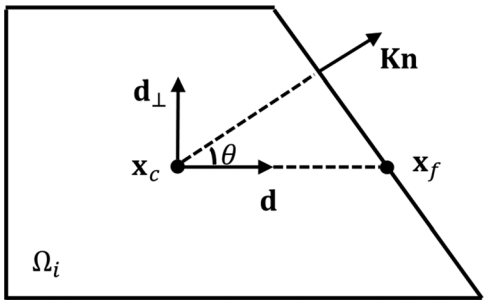

FIG. 3. Calculation of the degree of grid non-K-orthogonality for a cell-face pair.

one cell centroid and two face centroids. Darcy's law is then applied to compute the fluxes through the two corresponding sub-interfaces. For example, pressure in sub-region 1-A-O-D is approximated using pressure values at cell centroid $\mathbf{x}_1$ and face centroids $\mathbf{x}_A$, $\mathbf{x}_D$. Then fluxes through sub-interfaces OA and OD can be computed. Similarly, the calculation can be performed in the other three sub-regions. Finally, flux continuity condition is imposed on all the sub-interfaces to eliminate the auxiliary unknowns and the final flux approximation involves pressure values at the cell centroids only. For notation brevity, we will henceforth refer to the MPFA-O method as MPFA.

We choose the water pressure p_w and water saturation S_w as our primary unknowns and the CO_2 phase pressure and saturation are calculated by using the constraint equation (3). The system of nonlinear discrete equations at each time step are then linearized by using the Newton–Raphson nonlinear solver to advance the solutions to the next time step. In the following numerical experiments, we set the tolerance of the nonlinear solver to 1×10^{-5} and the allowed maximum number of nonlinear iterations to 25 for a given time step size. The time step size is adjusted dynamically during iterations: if the nonlinear solver fails to converge within 25 iterations, the time step size is cut in half.

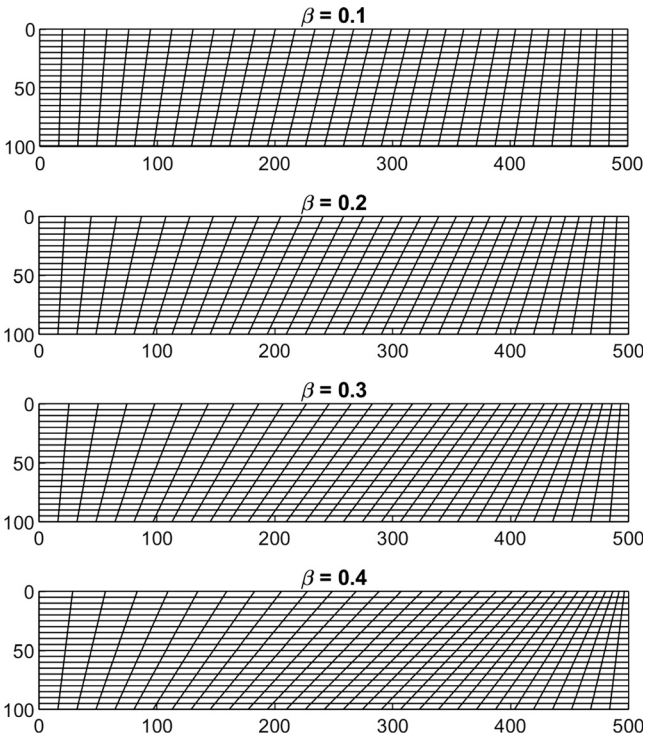

FIG. 4. Example inclined grid.

B. Quantification of grid non-K-orthogonality

As mentioned before, the TPFA method is only consistent for K-orthogonal grid. When the grid is non-K-orthogonal, the TPFA method incurs an $\mathcal{O}(1)$ error, i.e., the error does not decrease with grid refinement. However, if a grid is close to being K-orthogonal, the error of using TPFA method may be acceptable in practice and the use of TPFA can still be justified considering its robustness and efficiency. Therefore, it is highly desirable to have a quantitative measure of the degree of non-K-orthogonality of a grid for a given permeability field. In this section, we propose such a measure in the form of a numerical index based on the derivation of the TPFA formulation.

Consider an arbitrary cell Ω_i shown in Fig. 3. Take the flux approximation for the rightmost face as an example. For ease of notation, we have dropped the subscripts of some of the variables in the figure. The centroids of the cell and the face are denoted by $\mathbf{x}_c$ and $\mathbf{x}_f$, respectively. The vector $\mathbf{d}$ is defined as $\mathbf{d} = \frac{\mathbf{x}_f - \mathbf{x}_c}{\|\mathbf{x}_f - \mathbf{x}_c\|}$ and $\mathbf{d}_\perp$ is the unit vector perpendicular to $\mathbf{d}$. The unit normal vector to the face is denoted by $\mathbf{n}$ and it points out of the cell. $\mathbf{K}$ is the constant permeability tensor of the cell. The product of $\mathbf{K}$ and $\mathbf{n}$ is often termed as the co-normal vector in the literature.[22] The angle between the co-normal vector and the vector $\mathbf{d}$ is θ. Assuming a linearly varying pressure inside the cell, the pressure gradient can be calculated as

$$\nabla p = p_1 \mathbf{d} + p_2 \mathbf{d}_\perp, \tag{10}$$

where p_1 can be determined from pressure at the point $\mathbf{x}_c$ and $\mathbf{x}_f$, and p_2 is some unknown constant. The flux flowing out of the cell through the face can be approximated as

$$F = -A\mathbf{K}\nabla p \cdot \mathbf{n} = -A\nabla p \cdot (\mathbf{K}\mathbf{n}), \tag{11}$$

where A is the face area and the property of $\mathbf{K}$ being a symmetric tensor is utilized. Inserting Eq. (10) into (11) leads to

$$F = -A(p_1 \mathbf{d} + p_2 \mathbf{d}_\perp) \cdot \mathbf{K}\mathbf{n} = -p_1 A \mathbf{d} \cdot \mathbf{K}\mathbf{n} - p_2 A \mathbf{d}_\perp \cdot \mathbf{K}\mathbf{n}. \tag{12}$$

The magnitude of the two terms on the right-hand side of Eq. (12) can be calculated as

TABLE I. Phase and rock properties.

CO_2 phase density at reference condition	505.7 kg/m^3
Water phase density at reference condition	1000 kg/m^3
CO_2 phase compressibility	9.02×10^{-8} Pa^{-1}
Water phase compressibility	2.90×10^{-10} Pa^{-1}
Rock compressibility	4.35×10^{-10} Pa^{-1}
CO_2 phase viscosity	3.76×10^{-5} Pa s
Water phase viscosity	8.00×10^{-4} Pa s

04 September 2025 09:47:42

Published under an exclusive license by AIP Publishing

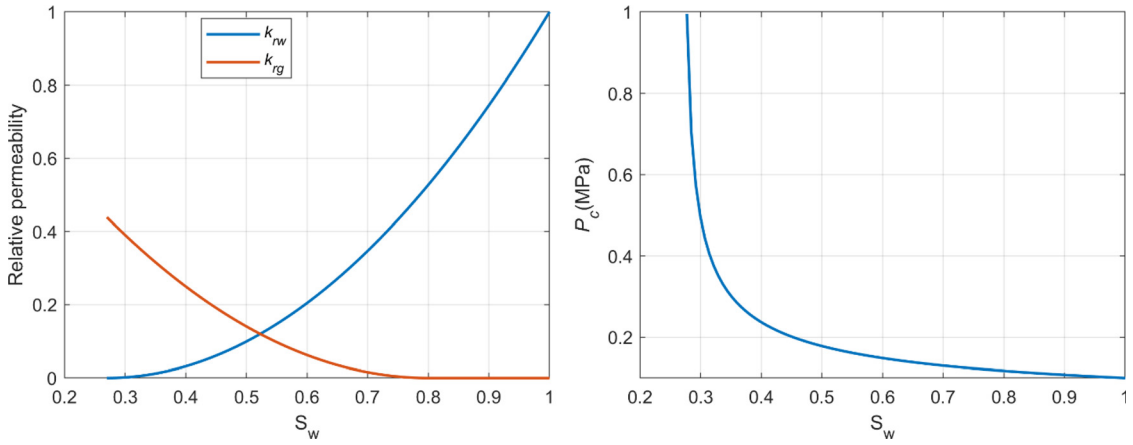

FIG. 5. Relative permeability curve (left) and capillary pressure curve (right).

$$
\begin{aligned}
|-p_1 A\mathbf{d}\cdot\mathbf{Kn}| &= |p_1|\cdot A\cdot\|\mathbf{Kn}\|\cdot\left|\cos(\theta)\right| \\
|-p_2 A\mathbf{d}_{\perp}\mathbf{Kn}| &= |p_2|\cdot A\cdot\|\mathbf{Kn}\|\cdot\left|\cos\left(\frac{\pi}{2}-\theta\right)\right| \\
&= |p_2|\cdot A\cdot\|\mathbf{Kn}\|\cdot\left|\sin(\theta)\right|. \qquad (13)
\end{aligned}
$$

The TPFA method drops the second term and keeps only the first term, thus introducing inconsistency. The error resulting from dropping the second term may be large or small depending on the relative magnitude of the two terms. Since the two coefficients p_1 and p_2 are not known *a priori*, we only consider the quantities dependent on the grid geometry and permeability field and define the degree of grid non-K-orthogonality for this pair of cell-face as

$$
\begin{aligned}
\eta_f &= \frac{A\cdot\|\mathbf{Kn}\|\cdot\left|\sin(\theta)\right|}{A\cdot\|\mathbf{Kn}\|\cdot\left|\cos(\theta)\right|+A\cdot\|\mathbf{Kn}\|\cdot\left|\sin(\theta)\right|} \\
&= \frac{\left|\sin(\theta)\right|}{\left|\cos(\theta)\right|+\left|\sin(\theta)\right|}. \qquad (14)
\end{aligned}
$$

The value of η_f lies in the interval [0, 1]. When the grid is K-orthogonal, the co-normal vector **Kn** is parallel to the vector **d** and η_f becomes zero. A high value of η_f indicates a large degree of grid non-K-orthogonality. Finally, the degree of grid non-K-orthogonality η for the whole grid is calculated by taking the mean of the η_f values for all the cell-face pairs in the grid

$$
\eta = \frac{1}{n_f}\sum_{f=1}^{n_f}\eta_f, \qquad (15)
$$

where n_f is the total number of cell-face pairs in the grid. Note that this numerical index η is only dependent on the grid geometry and the permeability tensor field and it can be calculated easily even for very complex grids seen in industry-standard simulations. We remark here that in addition to the grid geometry and permeability tensors, the numerical solution errors using TPFA method are also dependent on the actual flow scenarios. For example, if the flow is purely horizontal in Fig. 3, the coefficient p_2 in Eq. (10) is 0 and the TPFA flux approximation becomes consistent despite the grid non-K-orthogonality,

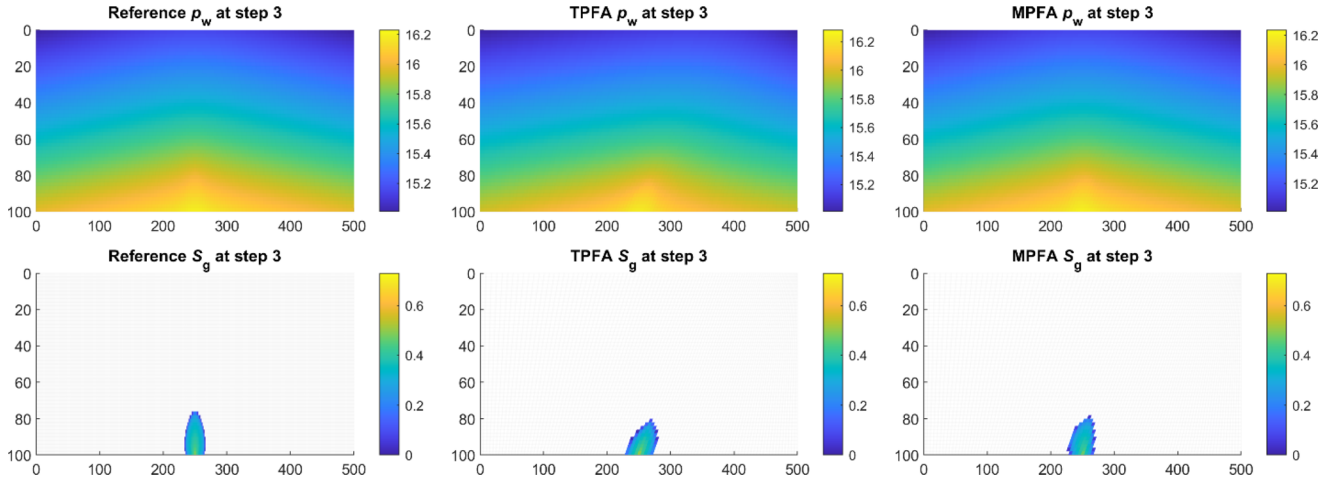

FIG. 6. Water pressure p_w in MPa (first row) and CO_2 saturation S_g(second row) at time $t = 30.4$ days (time step 3). From left to right: reference solution, TPFA solution and MPFA solution.

04 September 2025 09:47:42

Published under an exclusive license by AIP Publishing

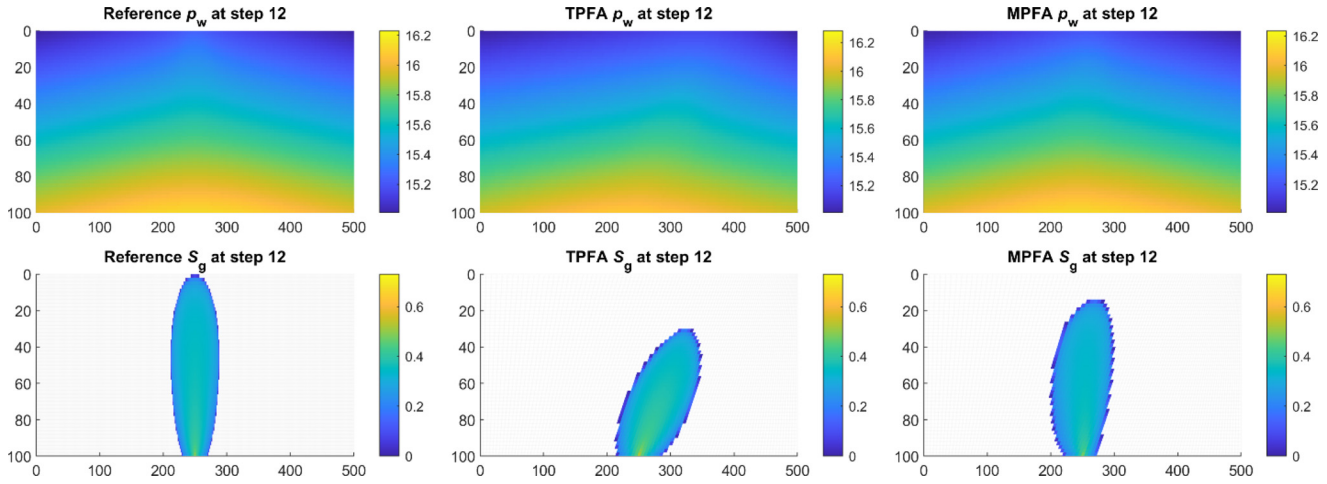

FIG. 7. Water pressure p_w in MPa (first row) and CO_2 saturation S_g(second row) at time $t = 304.37$ days (time step 12). From left to right: reference solution, TPFA solution and MPFA solution.

which is the so-called "false positive" for flow along the strata in Ref. 14. However, since the actual flow scenarios are not known *a priori* and they can also change as the flow driven mechanism changes, wo do not consider the "false positive" case as a deficiency of any static grid quality measures.

IV. RESULTS AND DISCUSSION

Numerical experiments were performed to evaluate the migration behavior of the CO_2 plume under different conditions. All examples are implemented within the framework of the open-source MATLAB Reservoir Simulation Toolbox (MRST).[11] We consider a 2D sector model that is 500 m in length and 100 m in depth with unit thickness. The domain was initially filled with brine at hydrostatic conditions with a reference pressure of 15 MPa at the top. The top and bottom of the domain are closed while the lateral boundaries are open to flow with pressure on the lateral boundaries equal to the initial hydrostatic pressure throughout the simulation. Supercritical CO_2 was injected at the bottom center at a rate of 0.05 pv/year. We modeled two years of CO_2 injection and two years of post-injection period. The two years of injection period was discretized into 26 times steps and the time step size was ramped up geometrically from approximately 7.6 to 30.4 days using the *rampupTimesteps* function in MRST. The two years of post-injection period was discretized eight time steps equally with the time step size of about 91.3 days. A non-orthogonal inclined grid of dimension 101×50 (101 cells in the horizontal direction and 50 cells in the vertical direction) was used to mimic the effect of faults on the meshing of the computational domain. The inclined grid is

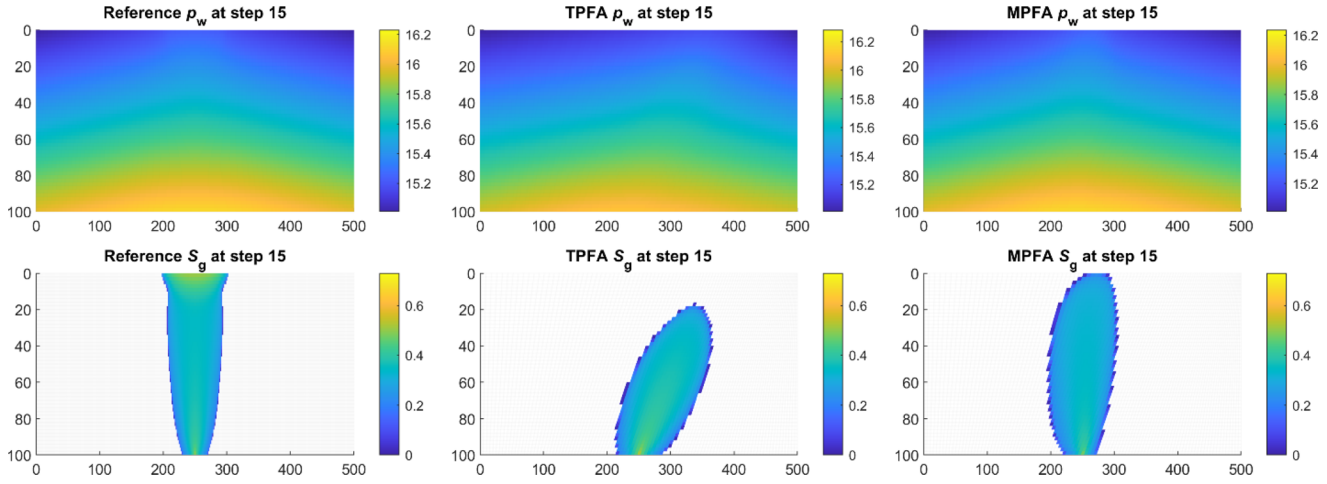

FIG. 8. Water pressure p_w in MPa (first row) and CO_2 saturation S_g (second row) at time $t = 395.7$ days (time step 15). From left to right: reference solution, TPFA solution and MPFA solution.

04 September 2025 09:47:42

Published under an exclusive license by AIP Publishing

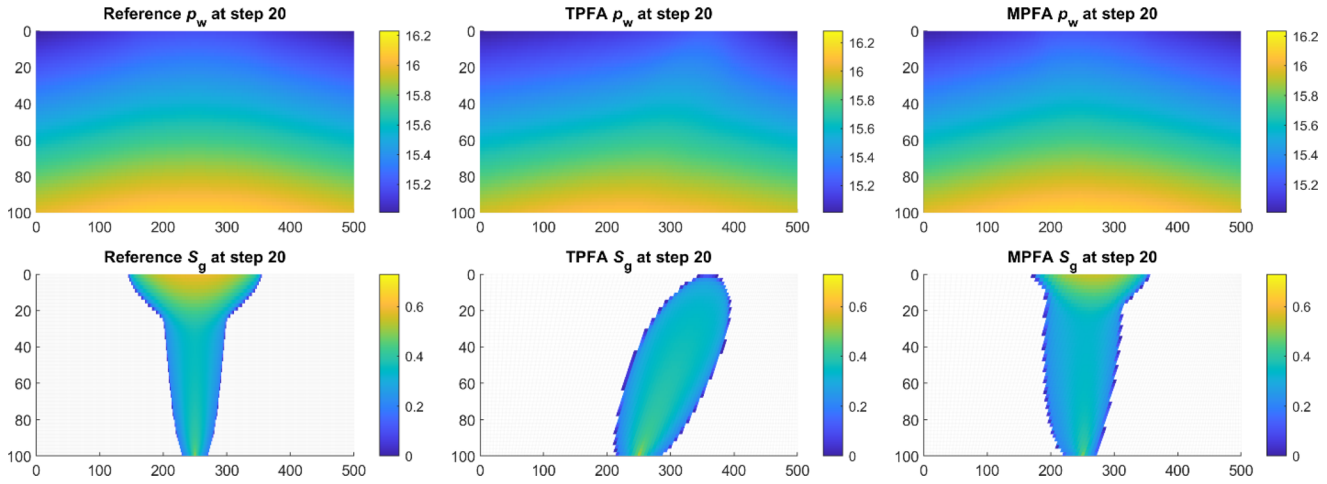

FIG. 9. Water pressure p_w in MPa (first row) and CO_2 saturation S_g (second row) at time $t = 547.9$ days (time step 20). From left to right: reference solution, TPFA solution and MPFA solution.

generated by changing the coordinates x, y of the nodes of a Cartesian grid on the domain $[0, 2] \times [0, 1]$ using the following equation

$$\tilde{x} = 2\Big(x + \beta\big(1 - (x-1)^2\big)(1-y)\Big), \tag{16}$$

where $\tilde{x}$ is the changed coordinate of the grid. The changed coordinates are then scaled to the actual reservoir size. Figure 4 shows an example grid of dimension 31×20 for clearer visualization. The degree of inclination of the grid was controlled by a factor β. As the value of β increases, the grid becomes progressively more inclined toward the east. The CO_2 properties were taken from the CO_2 lab of MRST. The reference pressure and temperature were set as 15 MPa and 70 °C, respectively. Table I lists other properties of the supercritical CO_2 phase and the resident brine phase. The Brooks–Corey type of relative permeability model was used to model water-supercritical CO_2 two phase flow where the irreducible water saturation, residual CO_2 saturation and Corey exponent are set as 0.27, 0.2, and 2, respectively. The Corey type of capillary model was used to model capillary pressure with pore-size distribution index set as 2. The left of Fig. 5 shows the relative permeability curves and an example capillary curve with entry pressure $p_e = 0.1$ MPa is shown on the right. We considered the cases of homogeneous permeability, layered permeability and heterogeneous permeability field. For comparison purposes, a reference solution was obtained by using the TPFA method to solve the numerical model on a fine Cartesian grid of dimension 321×50 for which the TPFA method is consistent. Because the cells of the reference fine grid do not align with the cells of the coarse inclined grid, when comparing the TPFA and MPFA solutions on the inclined grid with the reference solution, for each cell of the inclined grid, we find in the reference grid

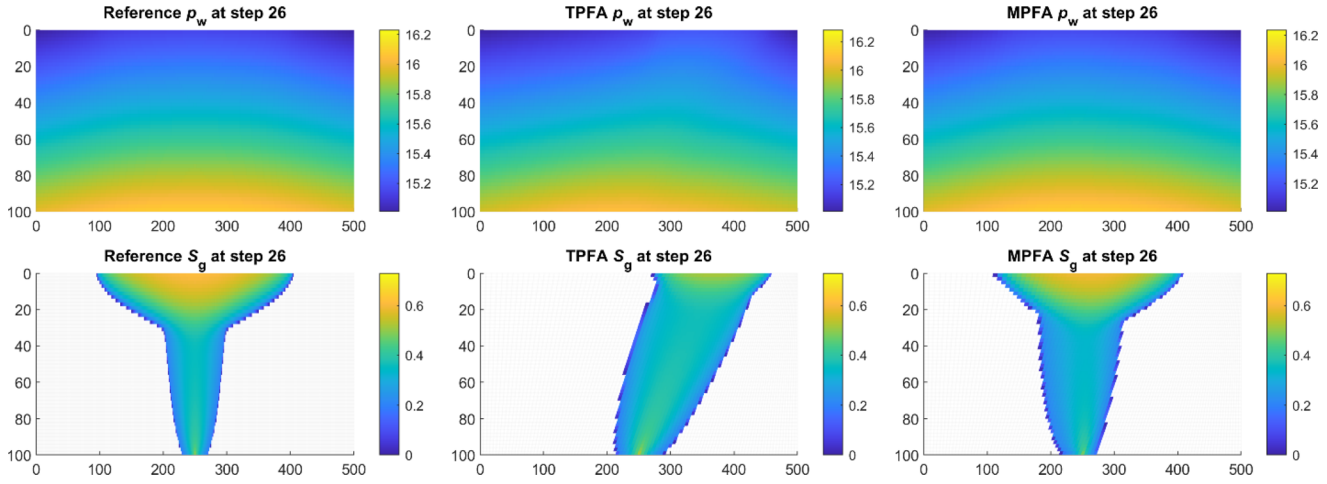

FIG. 10. Water pressure p_w in MPa (first row) and CO_2 saturation S_g (second row) at time $t = 730.5$ days (time step 26). From left to right: reference solution, TPFA solution and MPFA solution.

04 September 2025 09:47:42

Published under an exclusive license by AIP Publishing

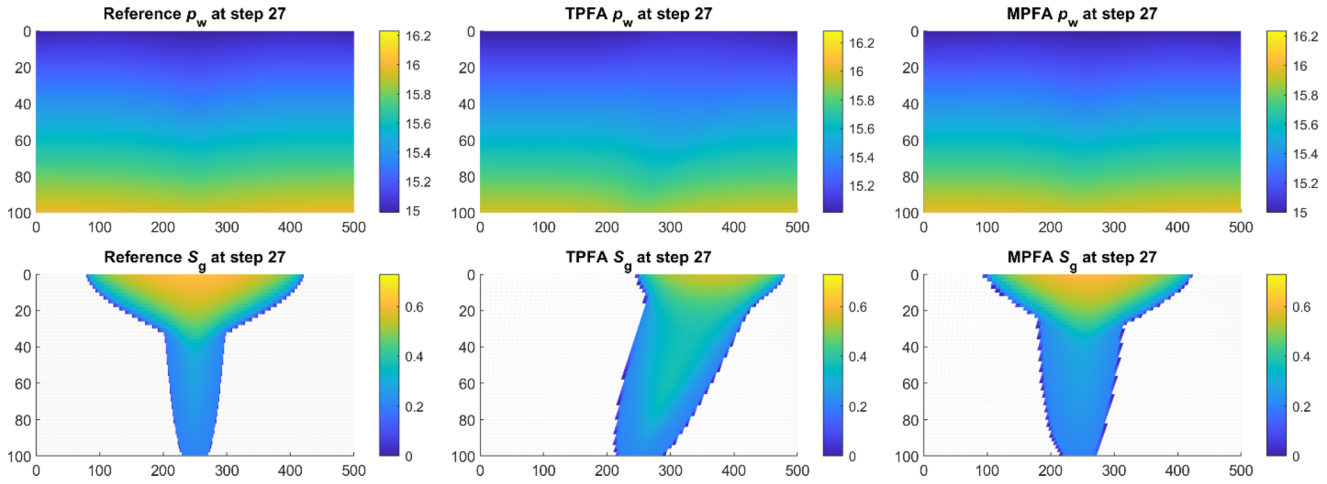

FIG. 11. Water pressure p_w in MPa (first row) and CO_2 saturation S_g (second row) at time $t = 821.8$ days (time step 27). From left to right: reference solution, TPFA solution and MPFA solution.

the cell whose centroid is closest to the cell and take its pressure and saturation values as reference solutions. To quantify the pressure solution errors at time step t, the mean relative error metric is used and defined as follows:

$$e_p^t = \frac{1}{n_c}\sum_{i=1}^{n_c}\frac{|p_{w,i}^t - \hat{p}_{w,i}^t|}{p_{w,i}^t}, \tag{17}$$

where n_c is the number of grid blocks; $p_{w,i}^t$ and $p_{w,i}^t$ are the reference pressure solution and TPFA/MPFA pressure solution at grid block i at time step t, respectively. The overall pressure solution error is calculated by averaging the pressure solution errors over all time steps

$$e_p = \frac{1}{n_t}\sum_{t=1}^{n_t} e_p^t. \tag{18}$$

To quantify the CO_2 gas saturation solution errors, the plume saturation error introduced in Ref. 29 is used and defined as

$$e_s^t = \frac{1}{\sum_{i=1}^{n_c} I_i^t}\sum_{i=1}^{n_c} I_i^t\left|S_{g,i}^t - \hat{S}_{g,i}^t\right|$$
$$I_i^t = 1 \text{ if } \left(S_{g,i}^t > 0.01\right) \cup \left(\hat{S}_{g,i}^t > 0.01\right), \tag{19}$$

where $S_{g,i}^t$ and $\hat{S}_{g,i}^t$ denote reference gas saturation solution and TPFA/MPFA gas saturation solution at grid block i at time step t, respectively. $I_i^t = 1$ indicates that either the reference gas saturation solution or the TPFA/MPFA solution is greater than a small threshold value (0.01 here) and $I_i^t = 0$ otherwise. As noted in Ref. 10, this plume saturation error metric focuses on the accuracy within the CO_2 plume and therefore provides a more strict metric to evaluate the CO_2 gas saturation

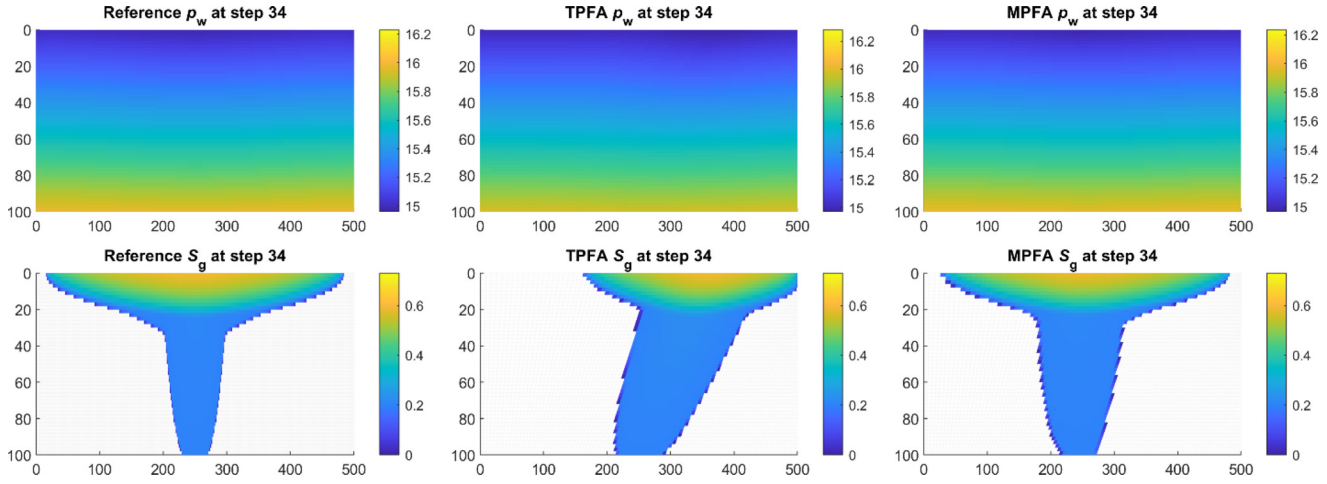

FIG. 12. Water pressure p_w in MPa (first row) and CO_2 saturation S_g (second row) at end of simulation (time step 34). From left to right: reference solution, TPFA solution and MPFA solution.

04 September 2025 09:47:42

Published under an exclusive license by AIP Publishing

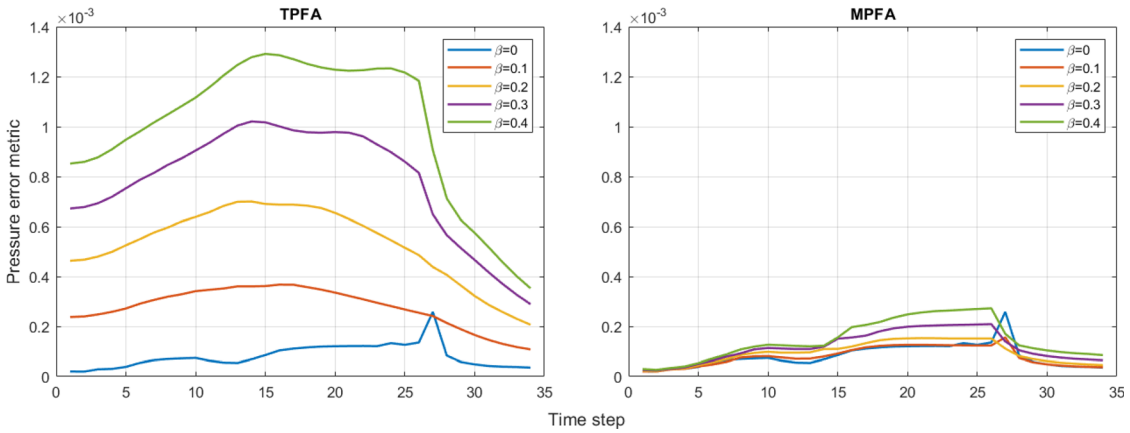

FIG. 13. Pressure error metric at each time step for TPFA (left) and MPFA (right) for case 1.

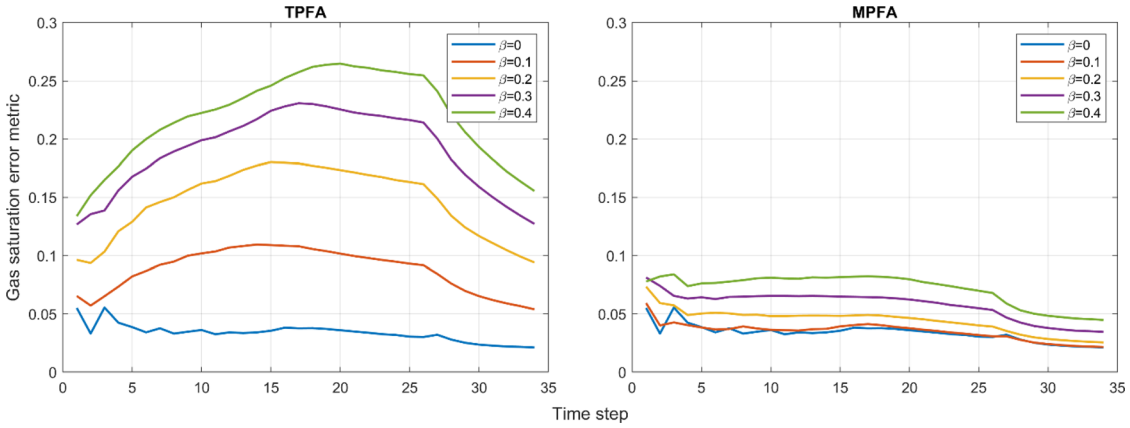

FIG. 14. CO_2 saturation error metric at each time step for TPFA (left) and MPFA (right) for case 1.

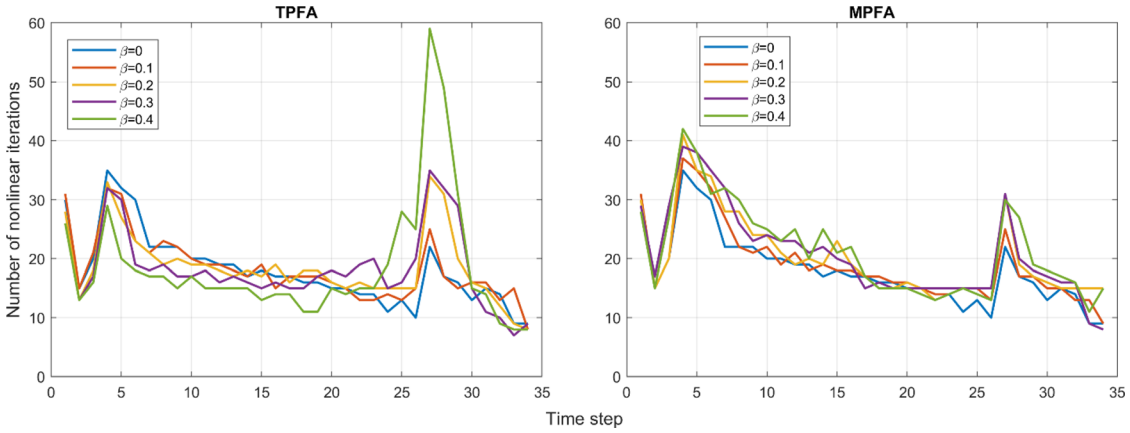

FIG. 15. Number of nonlinear Newton–Raphson iteration at each time step for case 1.

04 September 2025 09:47:42

Published under an exclusive license by AIP Publishing

TABLE II. Pressure and CO_2 saturation error metrics averaged over all time step and the total number of nonlinear iterations for TPFA and MPFA methods under different β values.

		e_p		e_s		n_{iter}	
β	η	TPFA	MPFA	TPFA	MPFA	TPFA	MPFA
0.0	0.0	0.0802×10^{-3}	0.0802×10^{-3}	0.0337	0.0337	614	614
0.1	0.1392	0.2775×10^{-3}	0.0794×10^{-3}	0.0878	0.0350	621	651
0.2	0.2396	0.5322×10^{-3}	0.0937×10^{-3}	0.1464	0.0442	633	693
0.3	0.3162	0.7836×10^{-3}	0.1187×10^{-3}	0.1846	0.0579	626	706
0.4	0.3767	1.000×10^{-3}	0.1442×10^{-3}	0.2191	0.0716	635	728

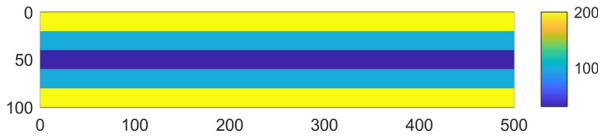

FIG. 16. Layered permeability configuration for case 2.

solution. Similarly, the overall gas saturation solution error is calculated by averaging the gas saturation solution errors over all time steps

$$e_s = \frac{1}{n_t}\sum_{t=1}^{n_t} e_s^t. \tag{20}$$

A. Case 1: Homogeneous permeability

In this first case, we consider a homogeneous permeability of 100 md and a constant porosity of 0.25 and run the numerical experiments for grids with different degrees of inclination by varying the β values. Figures 6–10 show five snapshots of water pressure and gas saturation of the reference solution, TPFA solution and MPFA solution during the injection period while two snapshots of the corresponding solutions during post-injection period are given in Figs. 11 and 12. The TPFA and MPFA solutions are for the grid with $\beta = 0.4$. Compared to the reference solution, both TPFA and MPFA methods suffer from the grid non-orthogonality effect even though the MPFA method is supposed to consistent for general non-orthogonal grid, but the MPFA solution is indeed much closer to the reference solution than the TPFA method in general. A closer inspection of the pressure solutions reveals that the effect of grid inclination on the TPFA method is more pronounced during the injection period than the post injection period: the pressure profiles of the TPFA method during the injection period are obviously non-symmetric compared to the reference solution and the MPFA solution, but the difference becomes indistinguishable during the post-injection period. When it comes to the CO_2 saturation solution, the differences among the TPFA solution, MPFA solution and the reference solution are more significant. The CO_2 saturation profile of the TPFA method is consistently non-symmetric for all time steps while the MPFA solution gradually becomes more symmetric over time and is closer and closer to the reference solution. Figure 7 shows that the reference solution suggests that the CO_2 plume rises to the top of the domain at about 304.37 days. Figures 8 and 9 show that the corresponding

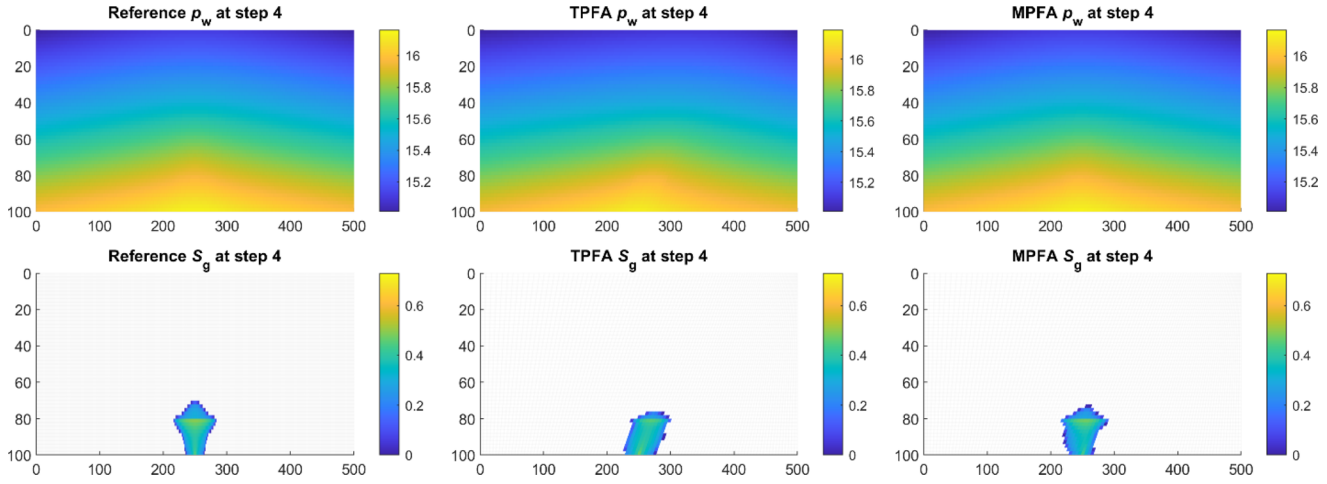

FIG. 17. Water pressure p_w in MPa (first row) and CO_2 saturation S_g (second row) at time $t = 60.87$ days (time step 4). From left to right: reference solution, TPFA solution and MPFA solution.

04 September 2025 09:47:42

Published under an exclusive license by AIP Publishing

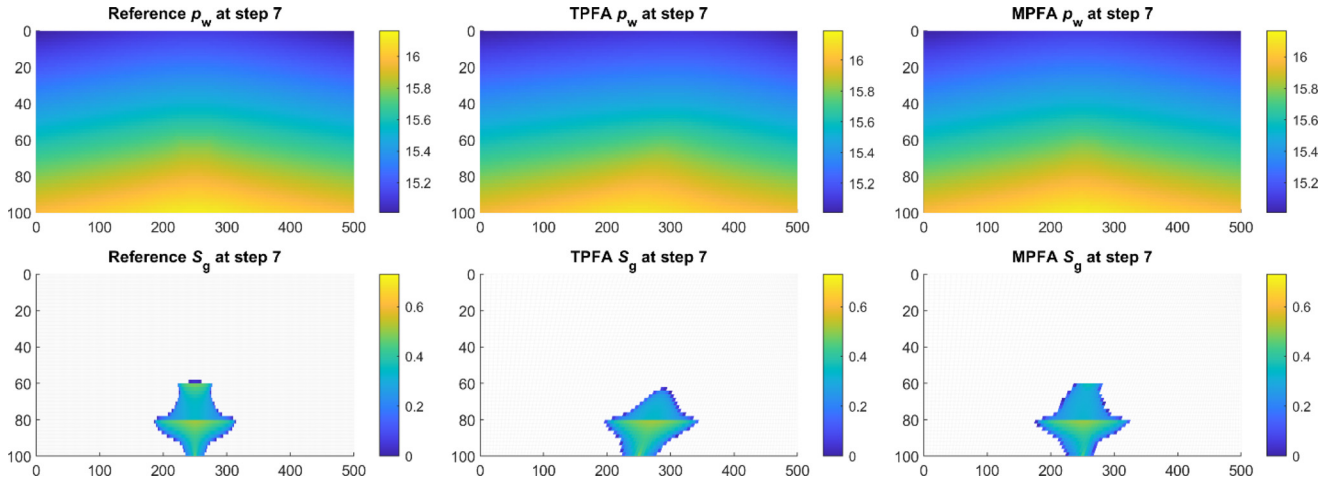

FIG. 18. Water pressure p_w in MPa (first row) and CO_2 saturation S_g (second row) at time $t = 152.18$ days (time step 7). From left to right: reference solution, TPFA solution and MPFA solution.

time suggested by the TPFA and MPFA solution is around 547.9 and 395.7 days, respectively, demonstrating again that the MFPA solution is in closer agreement with the reference solution. It must be noted, however, that the exact timing of CO_2 plume reaching to the top cannot be determined exactly because of the discrete nature of time step of the numerical simulations. Therefore, the actual difference of timing for TPFA and MPFA method compared to the reference solution may be smaller as the CO_2 plume has already reached to the top by time step 15 (for MFPA method) and time step 20 (for TPFA method).

Figures 13 and 14 show the evolution of error metrics for various β values using the TPFA method and the MFPA method for the pressure solutions and CO_2 saturation solutions, respectively. It can be seen that as β value increases, meaning increasing degree of grid inclination, pressure and saturation errors also increase for both TPFA and MFPA method. A β value of 0 means that the grid is orthogonal and the corresponding errors are caused by the difference of grid resolution for the reference solution and the TPFA/MFPA solutions and the corresponding errors serve as baselines. The TPFA and MFPA solutions are identical for β value of 0 as the classical MPFA-O method degenerates to the TPFA method on K-orthogonal grids. The results further confirm that the errors are in general larger during the injection period and becomes smaller for the post-injection period. Moreover, the relative error of pressure solutions is quite small even for the TPFA solution, but its saturation errors are quite significant. Overall, the MFPA solutions are much more satisfactory, suggesting that a more advanced numerical discretization scheme is necessary if accurate track of the CO_2 plume is required on non-orthogonal grids. Figure 15 displays the number of nonlinear Newton–Raphson iterations at each time step with various β values for the TPFA and MPFA method. The results show that increasing the degree of grid inclination tends to increase the number of nonlinear iterations required for both methods, but the

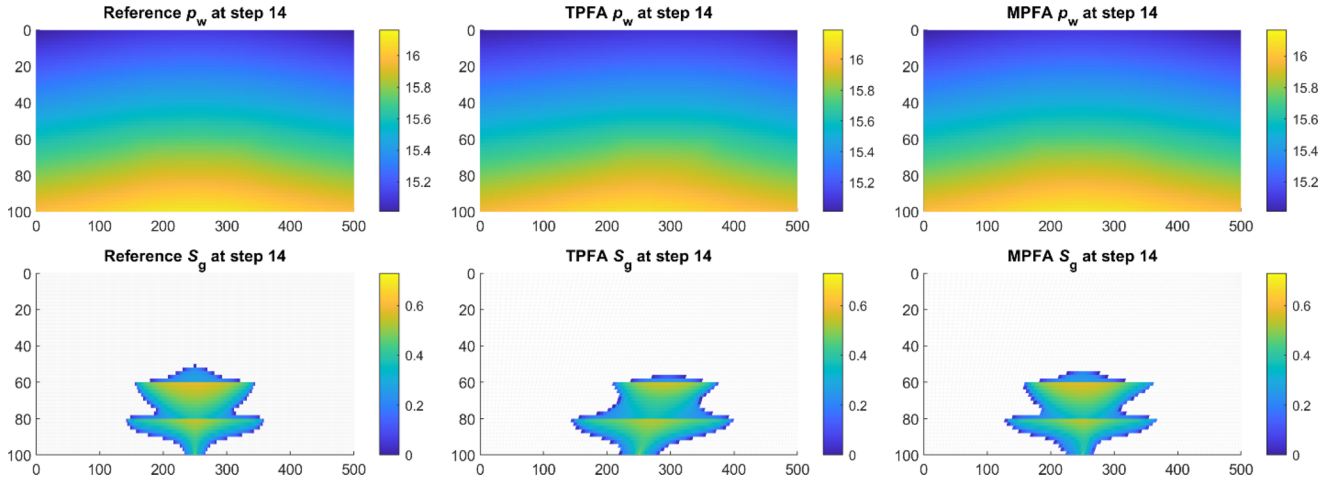

FIG. 19. Water pressure p_w in MPa (first row) and CO_2 saturation S_g (second row) at time $t = 365.24$ days (time step 14). From left to right: reference solution, TPFA solution and MPFA solution.

04 September 2025 09:47:42

Published under an exclusive license by AIP Publishing

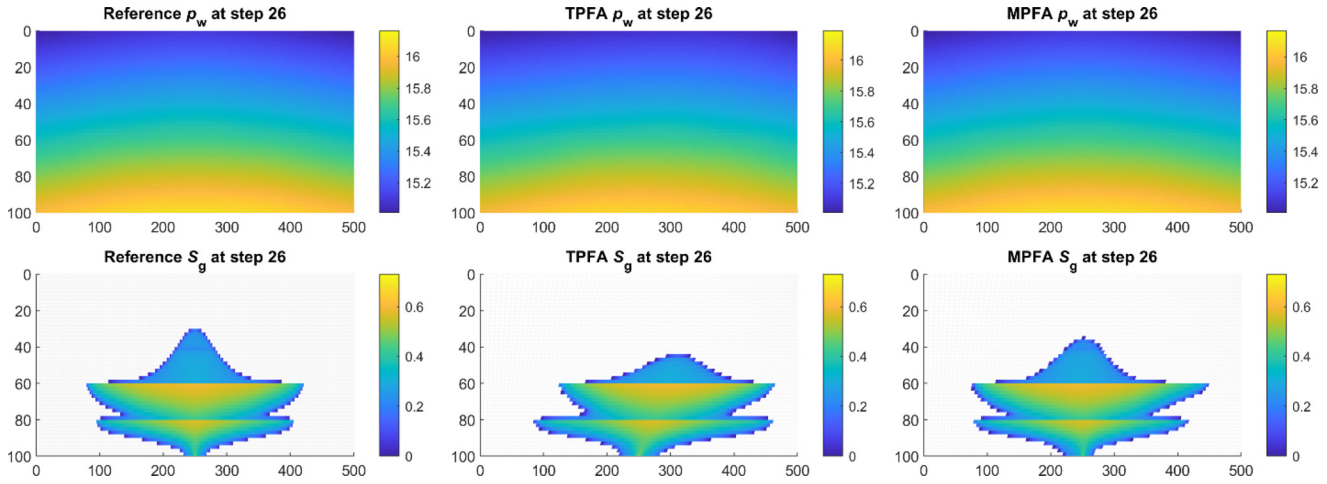

FIG. 20. Water pressure p_w in MPa (first row) and CO_2 saturation S_g (second row) at time $t = 730.49$ days (time step 26). From left to right: reference solution, TPFA solution and MPFA solution.

overall effect is minimal. The number of nonlinear iterations for MPFA method is generally greater than that of TPFA method and the difference increases as β increases. Combined with that fact that the linearized system of MPFA is denser than that of TPFA, it is computationally more expensive to solve. Finally, Table II lists the pressure and CO_2 saturation error metrics averaged over all time steps and the total number of nonlinear iterations required for TPFA and MPFA methods under different β values. From the error values listed in the table, we can see that for TPFA method, the overall pressure and CO_2 saturation errors for $\beta = 0.4$ increased about ten times and seven times, respectively, compared to the baseline errors ($\beta = 0$), while for MPFA method, both pressure and CO_2 saturation errors increased about two times, demonstrating that the MPFA method is much more robust against grid non-orthogonality than TPFA method. Also shown in the table are the degree of grid non-K-orthogonality values of η computed by using equation (15) proposed in Sec. III B. As expected, the solution error increases as the degree of the grid non-K-orthogonality increases for both TPFA and MPFA method.

B. Case 2: Layered permeability

In this second case we consider a layered permeability configuration shown in Fig. 16. The aquifer domain consists of five layers and the permeability values are 200, 100, 30, 100, and 200 md from the top layer to the bottom layer. The capillary entry pressure is set as 0.1 MPa for the layer with permeability of 100 md and the entry pressure for other layers is scaled by the reciprocal of the square root of its permeability. The low-permeability layer in the layer will impact the vertical migration the CO_2 plume. Figures 17–21 show several snapshots of pressure and CO_2 saturation profiles of the TPFA solution and MPFA solution for the grid with $\beta = 0.4$ along with the reference solution on

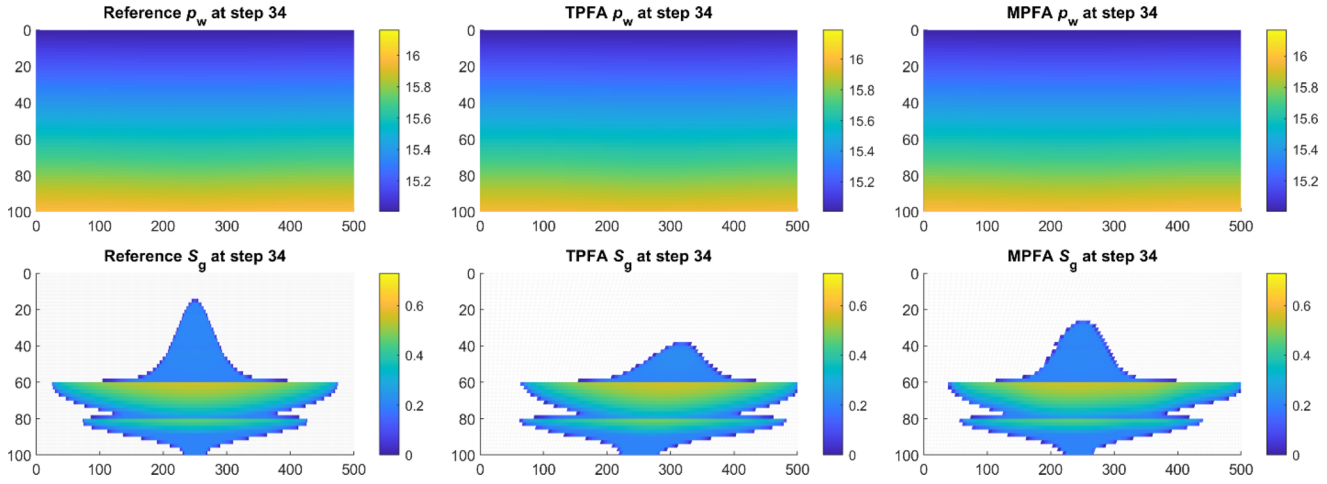

FIG. 21. Water pressure p_w in MPa (first row) and CO_2 saturation S_g (second row) at end of simulation (time step 34). From left to right: reference solution, TPFA solution and MPFA solution.

04 September 2025 09:47:42

Published under an exclusive license by AIP Publishing

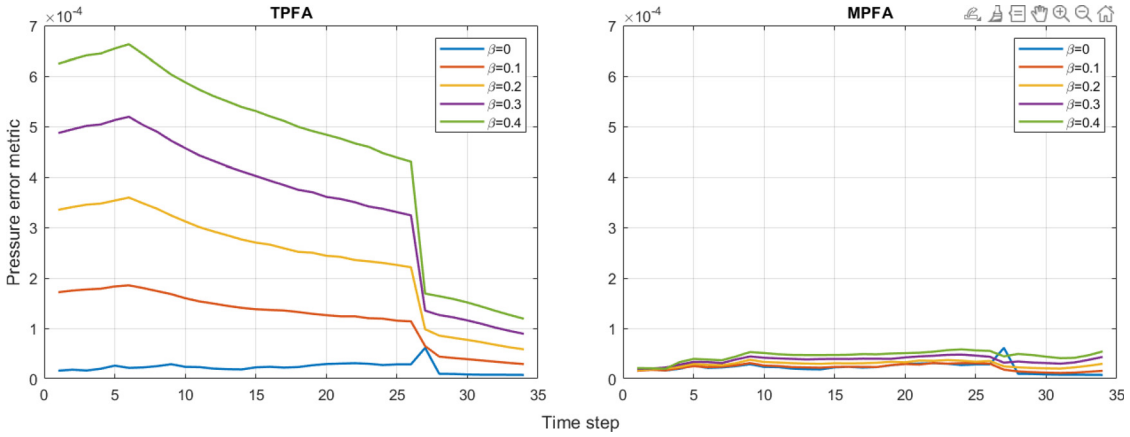

FIG. 22. Pressure error metric at each time step for TPFA (left) and MPFA (right) for case 2.

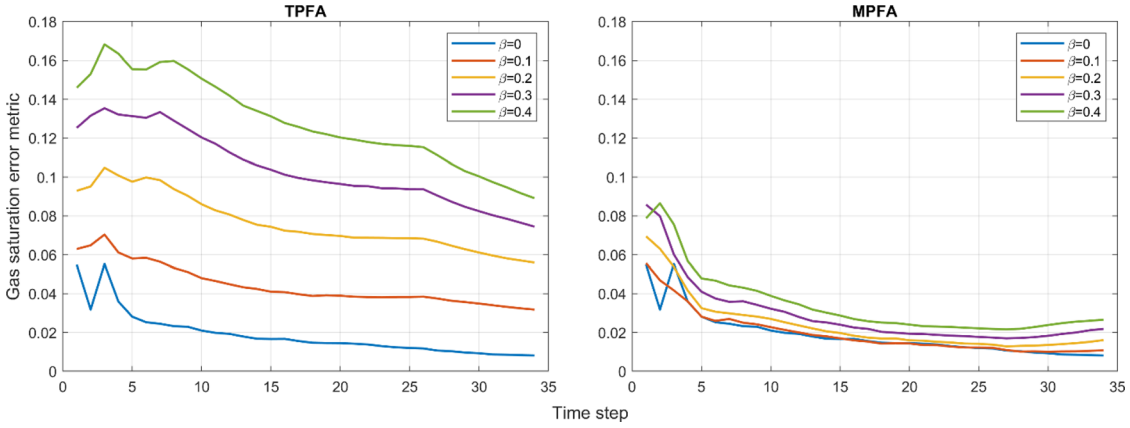

FIG. 23. CO_2 saturation error metric at each time step for TPFA (left) and MPFA (right) for case 2.

the Cartesian grid. Compared to the previous case, the layered permeability configuration has a significant impact on the migration of the CO_2 plume. The TPFA method, as expected, suffers from the grid non-orthogonality with both pressure and saturation solutions non-symmetrical. The MFPA method, on the other hand, tries to keep the solution symmetry and is affected to a much lesser degree by the non-orthogonal grid than the TPFA method. Figures 22 and 23 show the pressure and CO_2 saturation error metric for the TPFA and MPFA method on grids of varying degrees of inclination. Similar to the previous case, a higher degree of grid inclination leads to larger solution errors for both the TPFA and MPFA method, but the effect of grid non-orthogonality on TPFA method is much larger than MPFA

TABLE III. Pressure and CO_2 saturation error metrics averaged over all time step and the total number of nonlinear iterations for TPFA and MPFA methods under different β values.

		e_p		e_s		n_{iter}	
β	η	TPFA	MPFA	TPFA	MPFA	TPFA	MPFA
0.0	0.0	0.0218×10^{-3}	0.0218×10^{-3}	0.0188	0.0188	626	626
0.1	0.1392	0.1228×10^{-3}	0.0224×10^{-3}	0.0443	0.0194	648	650
0.2	0.2396	0.2376×10^{-3}	0.0287×10^{-3}	0.0766	0.0236	477	691
0.3	0.3162	0.3489×10^{-3}	0.0369×10^{-3}	0.1046	0.0291	462	661
0.4	0.3767	0.4546×10^{-3}	0.0453×10^{-3}	0.1286	0.0346	487	608

04 September 2025 09:47:42

Published under an exclusive license by AIP Publishing

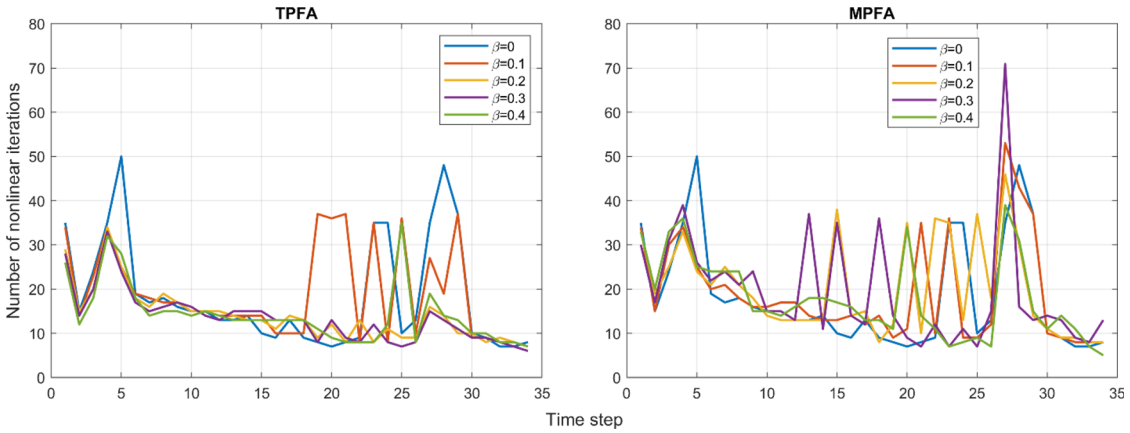

FIG. 24. Number of nonlinear Newton–Raphson iteration at each time step for case 2.

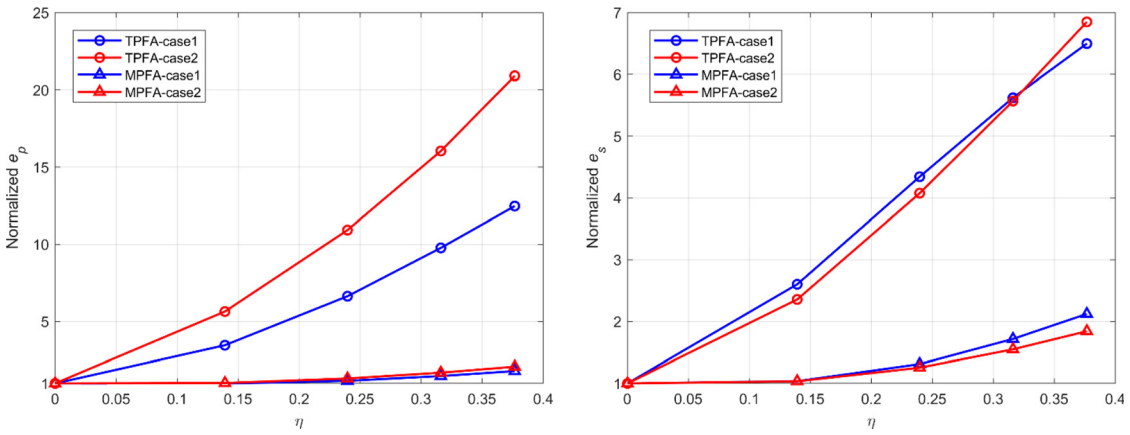

FIG. 25. Normalized pressure (left) and gas saturation (right) solution error metric as functions of the degree of grid non-K-orthogonality.

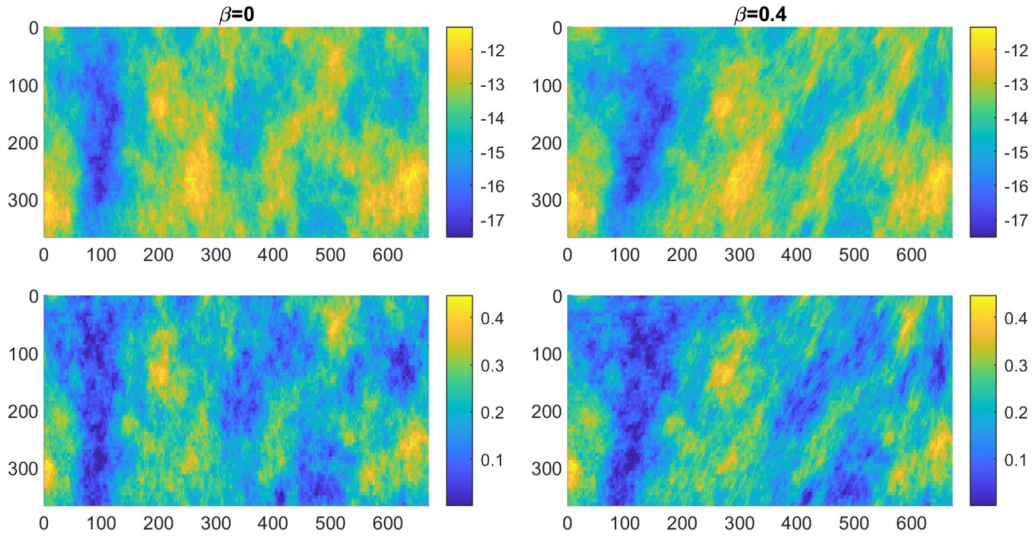

FIG. 26. Log permeability in SI unit (first row) and porosity (second row) of the first layer of the SPE10 dataset. The left column is the original data on the Cartesian grid and the second column is the result of direct mapping of the data to an inclined grid.

04 September 2025 09:47:42

Published under an exclusive license by AIP Publishing

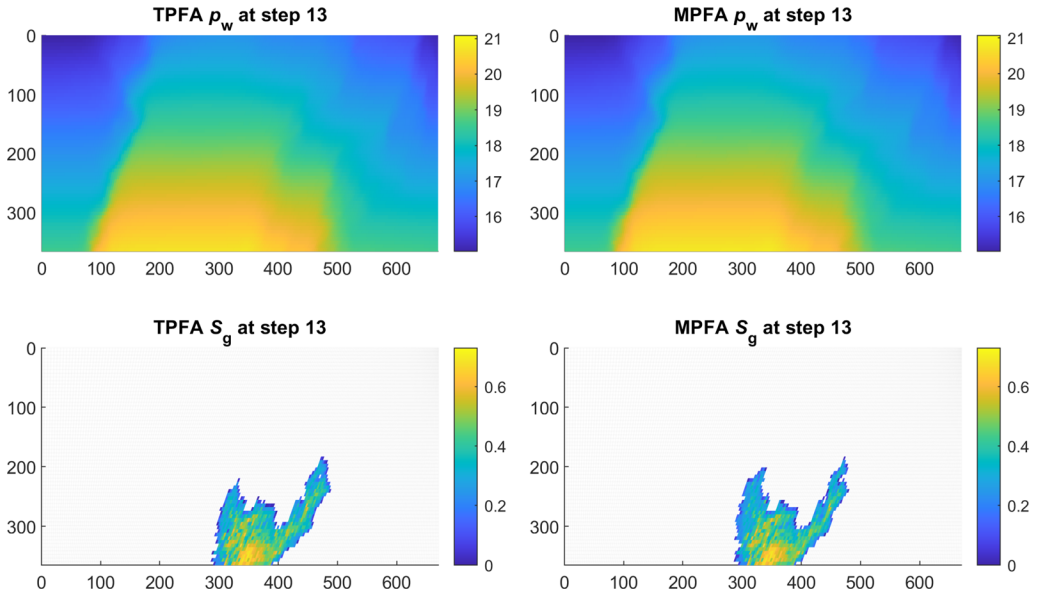

FIG. 27. Water pressure p_w in MPa (first row) and CO_2 saturation S_g (second row) at time $t = 334.81$ days (time step 13) using TPFA (left column) and MPFA method (right column).

method. By comparing Figs. 13 and 22, and Figs. 14 and 23, we can see that the magnitude of the solution errors of the TPFA and MPFA methods for this case study is smaller than the case 1 of homogeneous permeability, but this observation is misleading because the baseline errors ($\beta = 0$) are smaller for this case. Table III lists the pressure and CO_2 saturation error metrics averaged over all time step under different β values and we can see that pressure errors of TPFA for $\beta = 0.4$ increased approximately 20 times compared to baseline errors and the increase in CO_2 saturation errors is similar to the previous case, at about seven times, showing that the layer permeability configuration exacerbated the non-orthogonality issue suffered by TPFA method. The increase in MPFA solution errors remain about two times. Finally, Fig. 24 lists the number of nonlinear Newton–Raphson iterations at each time step for each grid using the TPFA and MPFA method and

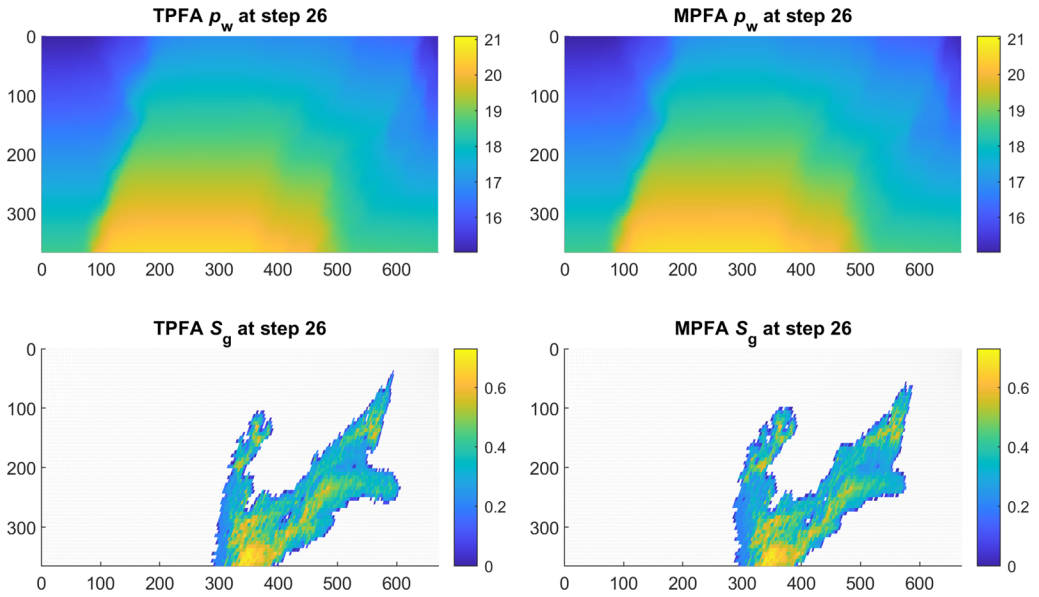

FIG. 28. Water pressure p_w in MPa (first row) and CO_2 saturation S_g (second row) at time $t = 730.49$ days (time step 26) using TPFA (left column) and MPFA method (right column).

04 September 2025 09:47:42

Published under an exclusive license by AIP Publishing

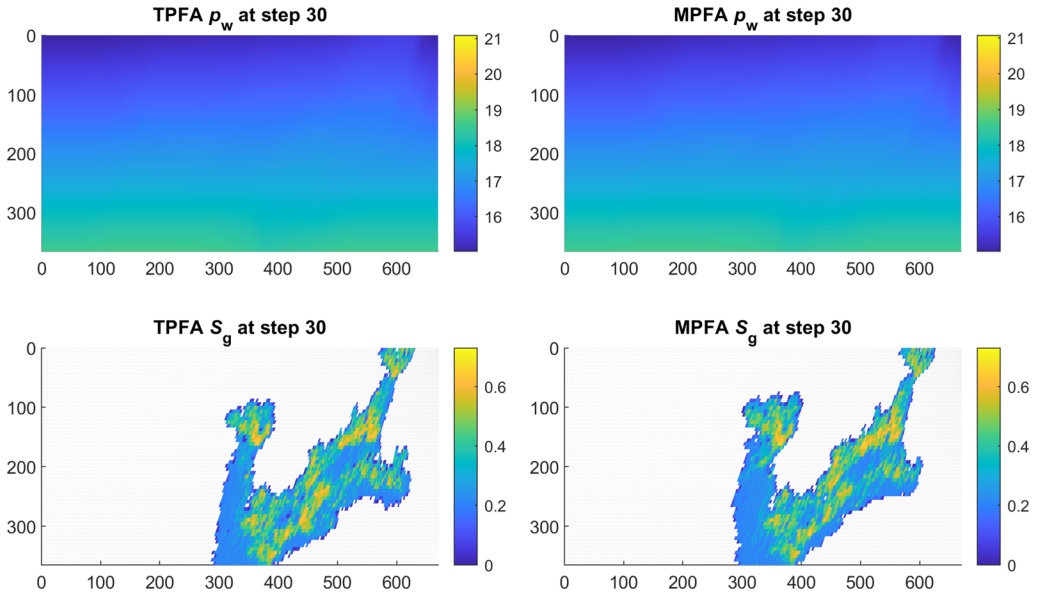

FIG. 29. Water pressure p_w in MPa (first row) and CO_2 saturation S_g (second row) at time t= 1095.7 days (time step 30) using TPFA (left column) and MPFA method (right column).

the total number nonlinear iterations are also listed in Table III. The MPFA method requires more nonlinear iterations at some time steps for certain grids, but there is no clear correlation between the degree of grid inclination and the number of nonlinear iterations for both methods, meaning a more inclined grid does not necessarily increase the number of nonlinear iterations as one may expect. Note that the degree of grid non-K-orthogonality η values shown in Table III are the same as the previous case. However, the magnitude of the solution errors in this case is different from the previous case, which is unsurprising since the baseline errors ($\beta = 0$, grid is K-orthogonal) are also different for the two cases. To compare the magnitude of the solution error metrics of the two cases, we normalize the solution error e_p and e_s by their respective baseline errors and plot the normalized solution errors vs the degree of grid non-K-orthogonality η in Fig. 25. We observe that with the exception of the pressure solutions for TPFA, the normalized solution errors are in general quite close for the two cases for any given degree of grid non-K-orthogonality η, demonstrating the potential usefulness of the proposed grid non-K-orthogonality index for evaluating solution accuracy in a general simulation study.

C. Case 3: Heterogeneous permeability

In this final case we consider a highly heterogeneous permeability field by taking the permeability and porosity values from the first layer of the SPE10 dataset. The original dataset populates a regular Cartesian grid. We take the permeability and porosity values and map them directly to our inclined grid. Figure 26 shows the original log permeability and porosity maps and the corresponding maps on the inclined grid with $\beta = 0.4$. This direct mapping of data from Cartesian grid to incline grid will change the overall distribution of the permeability and porosity values on the computational domain. Therefore, a reference solution using TPFA method on the Cartesian grid is not applicable and we only compare the pressure and saturation solution differences between the TPFA and MPFA method. To prevent numerical difficulties, a permeability threshold value of 1×10^{-6} md and a porosity threshold value of 1×10^{-3} are set. Permeability and porosity values smaller than the threshold values are set to the corresponding threshold values. The classical Leverett J function is used to model the heterogenous capillary pressure. The functional form of the dimensionless J function is given as

$$\begin{cases} J(S_{we}) = J_0 S_{we}^{-1/\lambda} \\ S_{we} = \dfrac{S_w - S_{wr}}{1 - S_{wr}} \end{cases}. \tag{21}$$

The capillary function is computed as

$$P_c(S_w) = J(S_{we}) \frac{\sigma \cos\theta}{\sqrt{k/\phi}}, \tag{22}$$

where J_0, λ, σ, θ are scaling constant, pore size distribution index, interfacial tension and contact angle, respectively. Their values are taken as 0.5, 2, 30 mN/m and 0° for this case study.

Figures 27 and 28 show two snapshots of water pressure, CO_2 gas saturation solutions using TPFA method and MPFA method for time step 13 and time step 26 (when the injection period ends), respectively, on the grid with $\beta = 0.4$, and Figs. 29 and 30 show two snapshots of corresponding solutions during the post injection period. A visual comparison shows that the pressure solutions of the TPFA method and the MPFA method are quite close to each other while the CO_2 plume solutions of the two methods share similar global transport pattern but differ locally. This is confirmed by a quantitative comparison between the TPFA and MPFA solutions shown in Fig. 31 where the mean relative difference of pressure solution and mean absolute CO_2 saturation solution at each time step for different grids are calculated and Table IV where the solution differences averaged over all time

04 September 2025 09:47:42

Published under an exclusive license by AIP Publishing

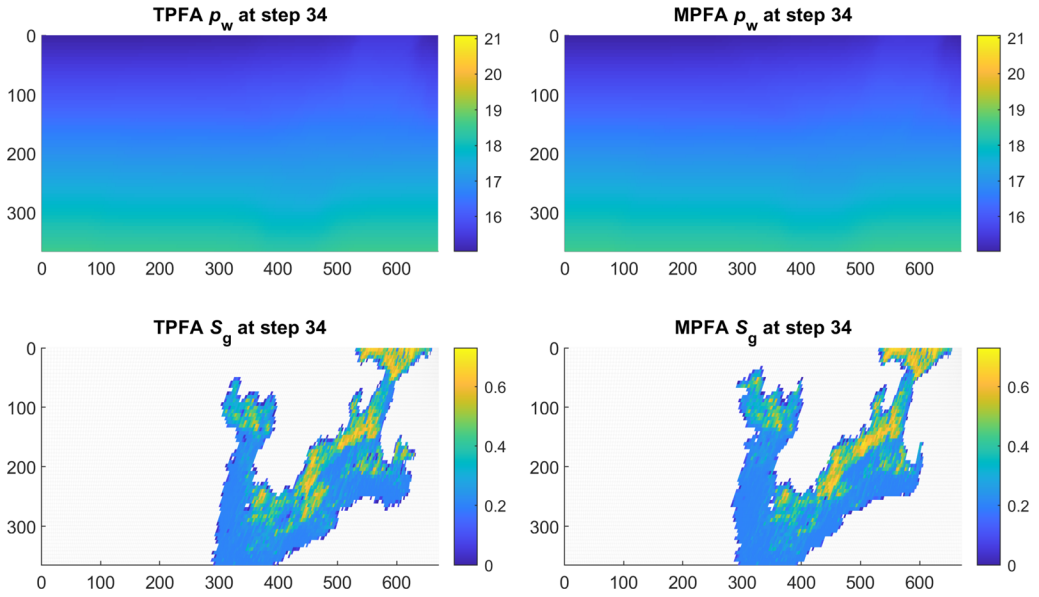

FIG. 30. Water pressure p_w in MPa (first row) and CO_2 saturation S_g (second row) at end of simulation (time step 34) using TPFA (left column) and MPFA method (right column).

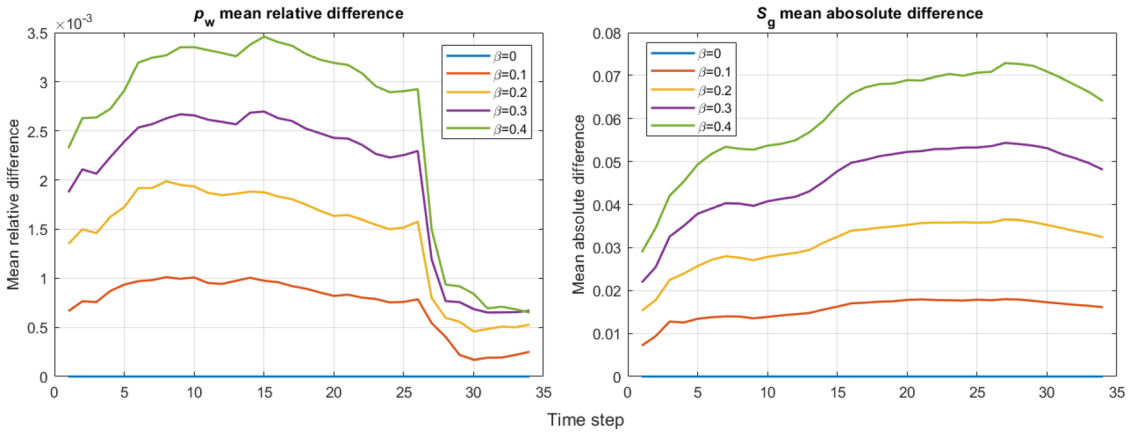

FIG. 31. Mean relative pressure solution difference (left) and mean absolute saturation solution difference (right) between TPFA and MPFA at each time step for grid with varying β values.

TABLE IV. Pressure and CO_2 saturation solution differences between TPFA and MPFA averaged over all time step and the total number of nonlinear iterations for TPFA and MPFA methods under different β values.

				n_{iter}	
β	η	ep	es	TPFA	MPFA
0.0	0.0	0	0	942	942
0.1	0.0570	0.0007	0.0156	1031	942
0.2	0.1067	0.0014	0.0312	975	964
0.3	0.1507	0.0020	0.0459	1014	1044
0.4	0.1898	0.0026	0.0608	1064	1038

steps are listed. The mean relative difference of pressure solution and mean absolute CO_2 saturation solution are calculated using Eqs. (17)–(20) with the reference solution in the equations replaced by MPFA solution. Even for the grid with the largest degree of inclination, the mean relative differences of pressure solutions are small and the mean absolute differences of saturation solutions remain smaller than 0.08. The degree of grid non-K-orthogonality η for the grids with different β values are shown in Table IV and we found that the largest degree of grid non-K-orthogonality for this case is less than 0.2, thus explaining the small difference between TPFA and MPFA solutions. The results further confirm the usefulness of the proposed grid non-K-orthogonality index. Finally, the number of nonlinear Newton–Raphson iterations for the two methods are shown in Fig. 32 and the total number

04 September 2025 09:47:42

Published under an exclusive license by AIP Publishing

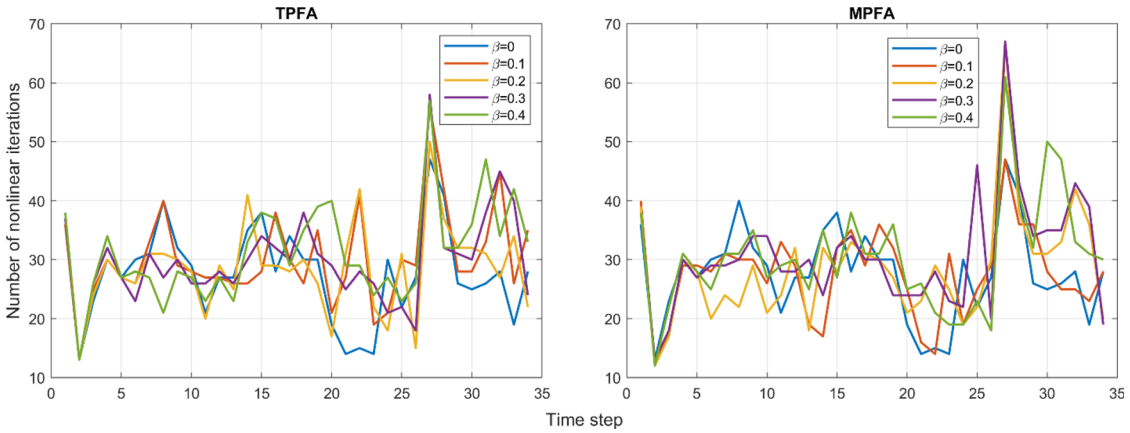

FIG. 32. Number of nonlinear Newton–Raphson iteration at each time step for case 3.

of nonlinear iterations are listed in Table IV. Because of the heterogeneity, the nonlinear solver requires a much greater number of iterations to converge compared to the previous two cases. Interestingly, the total number of nonlinear iterations for the MPFA method is smaller than TPFA for several grids in this case.

V. CONCLUSION

A numerical index is proposed in this work to quantify the degree of grid non-K-orthogonality and a series of numerical experiments of increasing complexity were conducted to systematically assess the effect of grid non-K-orthogonality on the solution accuracy of TPFA and MPFA methods in the context of CO_2 storage in saline aquifers and the following conclusions can be made: (1) Both the TPFA and MPFA method suffer from the grid non-K-orthogonality with increasing degree of grid non-K-orthogonality leading to larger errors for both the pressure and CO_2 saturation solutions despite the fact that MPFA method is consistent for general non-K-orthogonal grids. (2) The magnitude of solution errors of MPFA is significantly lower than that of TPFA for cases. (3) For the cases considered here, the errors of pressure solutions are generally quite small even for TPFA method, but substantial errors can be incurred using TPFA method when it comes to CO_2 saturation solution, suggesting advanced discretization method such as MFPA is needed if CO_2 plume is to be tracked accurately. (4) Layered permeability configurations can exacerbate the negative effect of grid non-K-orthogonality on TPFA solutions while MFPA method remains robust. (5) Grid non-K-orthogonality does not seem to have an obvious impact on the convergence of Newton–Raphson solver in terms of nonlinear iteration for both TPFA and MPFA method. Depending on the cases, the total number of nonlinear iterations may increase or decrease as the degree of grid non-K-orthogonality increases.

ACKNOWLEDGMENTS

This work was supported by the National Natural Science Foundation of China (Grant No. 52304030) and the Natural Science Foundation of Shandong Province, China (Grant No. ZR2023QA034).

AUTHOR DECLARATIONS

Conflict of Interest

The authors have no conflicts to disclose.

Author Contributions

Wenjuan Zhang: Conceptualization (equal); Data curation (equal); Formal analysis (equal); Funding acquisition (equal). **Kai Zhang:** Project administration (equal); Supervision (equal). **Mohammed Al Kobaisi:** Software (equal); Writing – review & editing (equal).

DATA AVAILABILITY

The data that support the findings of this study are available from the corresponding author upon reasonable request.

REFERENCES

[1]M. A. Celia, S. Bachu, J. M. Nordbotten, and K. W. Bandilla, "Status of CO_2 storage in deep saline aquifers with emphasis on modeling approaches and practical simulations," Water Resour. Res. **51**(9), 6846–6892, https://doi.org/10.1002/2015WR017609 (2015).
[2]Q. Wang, D. Zhang, Y. Li, C. Li, and H. Tang, "Numerical simulation study of CO_2 storage capacity in Deep Saline aquifers," Sci. Technol. Energy Transition **79**, 12 (2024).
[3]T. Akai, T. Kuriyama, S. Kato, and H. Okabe, "Numerical modelling of long-term CO_2 storage mechanisms in saline aquifers using the Sleipner benchmark dataset," Int. J. Greenhouse Gas Control **110**, 103405 (2021).
[4]X. Rao, X. He, Y. Xu, and H. Kwak, "Numerical simulation of carbon dioxide flooding in fractured reservoirs using generic projection-based embedded discrete fracture model," Phys. Fluids **36**(10), 106601 (2024).
[5]T. Urych, J. Chećko, M. Magdziarczyk, and A. Smoliński, "Numerical simulations of carbon dioxide storage in selected geological structures in northwestern Poland," Front. Energy Res. **10**, 827794 (2022).
[6]I. Sypchenko and A. Afanasyev, "CO_2 storage efficiency in saline aquifers: Insight from the numerical modeling of immiscible displacement," Phys. Fluids **36**(12), 126624 (2024).
[7]M. Hamed and E. Shirif, "Sustainable CO_2 storage assessment in saline aquifers using a hybrid ANN and numerical simulation model across different trapping mechanisms," Sustainability **17**, 2904 (2025).
[8]S. Mo, Y. Zhu, N. Zabaras, X. Shi, and J. Wu, "Deep convolutional encoder-decoder networks for uncertainty quantification of dynamic multiphase flow in heterogeneous media," Water Resour. Res. **55**(1), 703–728, https://doi.org/10.1029/2018WR023528 (2019).

04 September 2025 09:47:42

Published under an exclusive license by AIP Publishing

[9]G. Wen, Z. Li, K. Azizzadenesheli, A. Anandkumar, and S. M. Benson, "U-FNO—An enhanced Fourier neural operator-based deep-learning model for multiphase flow," Adv. Water Resour. **163**, 104180 (2022).
[10]X. Ju, F. P. Hamon, G. Wen, R. Kanfar, M. Araya-Polo, and H. A. Tchelepi, "Learning CO_2 plume migration in faulted reservoirs with Graph Neural Networks," Comput. Geosci. **193**, 105711 (2024).
[11]K.-A. Lie, *An Introduction to Reservoir Simulation Using MATLAB/GNU Octave: User Guide for the MATLAB Reservoir Simulation Toolbox (MRST)* (Cambridge University Press, Cambridge, 2019).
[12]H. Yamamoto and C. Doughty, "Investigation of gridding effects for numerical simulations of CO_2 geologic sequestration," Int. J. Greenhouse Gas Control **5**(4), 975–985 (2011).
[13]D. Gunasekera, J. Cox, and P. Lindsey, "The generation and application of K-orthogonal grid systems," in paper presented at the SPE Reservoir Simulation Symposium, Dallas, Texas, June 1997.
[14]I. Mishev and R. Rin, "Grid quality measures for PEBI grids," in *SPE Reservoir Simulation Conference* (SPE, 2021).
[15]P. H. Sammon, M. Kurihara, and L. Jialing, "Applying high-resolution numerical schemes in reservoirs described by complex corner-point grids," in *SPE Reservoir Simulation Symposium* (SPE, 2001).
[16]I. Aavatsmark, "An introduction to multipoint flux approximations for quadrilateral grids," Comput. Geosci. **6**(3), 405–432 (2002).
[17]M. G. Edwards and C. F. Rogers, "Finite volume discretization with imposed flux continuity for the general tensor pressure equation," Comput. Geosci. **2**(4), 259–290 (1998).
[18]W. Zhang and M. Al Kobaisi, "A simplified enhanced MPFA formulation for the elliptic equation on general grids," Comput. Geosci. **21**(4), 621–643 (2017).
[19]K. Lipnikov, G. Manzini, and M. Shashkov, "Mimetic finite difference method," J. Comput. Phys. **257**, 1163–1227 (2014).
[20]X. Yan, Z. Huang, J. Yao, Y. Li, and D. Fan, "An efficient embedded discrete fracture model based on mimetic finite difference method," J. Pet. Sci. Eng. **145**, 11–21 (2016).
[21]M. Schneider, B. Flemisch, and R. Helmig, "Monotone nonlinear finite-volume method for nonisothermal two-phase two-component flow in porous media," Int. J. Numer. Methods Fluids **84**(6), 352–381 (2017).
[22]W. Zhang and M. Al Kobaisi, "Cell-centered nonlinear finite-volume methods with improved robustness," SPE J. **25**(01), 288–309 (2020).
[23]J. E. Aarnes, T. Gimse, and K.-A. Lie, "An introduction to the numerics of flow in porous media using Matlab," in *Geometric Modelling, Numerical Simulation, and Optimization: Applied Mathematics at SINTEF*, edited by G. Hasle, K.-A. Lie, and E. Quak (Springer Berlin Heidelberg: Berlin, Heidelberg, 2007), pp. 265–306.
[24]J. M. Nordbotten and G. T. Eigestad, "Discretization on quadrilateral grids with improved monotonicity properties," J. Comput. Phys. **203**(2), 744–760 (2005).
[25]I. Aavatsmark, G. T. Eigestad, B. T. Mallison, and J. M. Nordbotten, "A compact multipoint flux approximation method with improved robustness," Numer. Methods Partial **24**(5), 1329–1360 (2008).
[26]H. A. Friis and M. G. Edwards, "A family of MPFA finite-volume schemes with full pressure support for the general tensor pressure equation on cell-centered triangular grids," J. Comput. Phys. **230**(1), 205–231 (2011).
[27]Q.-Y. Chen, J. Wan, Y. Yang, and R. T. Mifflin, "Enriched multi-point flux approximation for general grids," J. Comput. Phys. **227**(3), 1701–1721 (2008).
[28]G. T. Eigestad and R. A. Klausen, "On the convergence of the multi-point flux approximation O-method: Numerical experiments for discontinuous permeability," Numer. Methods Partial **21**(6), 1079–1098 (2005).
[29]G. Wen, Z. Li, Q. Long, K. Azizzadenesheli, A. Anandkumar, and S. M. Benson, "Real-time high-resolution CO_2 geological storage prediction using nested Fourier neural operators," Energy Environ. Sci. **16**(4), 1732–1741 (2023).

04 September 2025 09:47:42

Published under an exclusive license by AIP Publishing